

TOPICAL REVIEW • OPEN ACCESS

Mass transfer techniques for large-scale and high-density microLED arrays

To cite this article: Furong Chen *et al* 2022 *Int. J. Extrem. Manuf.* **4** 042005


View the [article online](#) for updates and enhancements.

You may also like

- [Integrated parabolic nanolenses on MicroLED color pixels](#)
Brandon Demory, Kunook Chung, Adam Katcher et al.
- [Significant reduction in sidewall damage related external quantum efficiency \(EQE\) drop in red InGaN microLEDs \(625 nm at 1 A cm⁻²\) with device sizes down to 3 μm](#)
Surjava Sanyal, Qinchen Lin, Timothy Shih et al.
- [Cathodoluminescence investigations of dark-line defects in platelet-based InGaN nano-LED structures](#)
Anders Gustafsson, Axel R Persson, Per O Å Persson et al.

Topical Review

Mass transfer techniques for large-scale and high-density microLED arrays

Furong Chen^{1,2,4}, Jing Bian^{1,2,3,4}, Jinlong Hu^{1,2}, Ningning Sun^{1,2}, Biao Yang^{1,2}, Hong Ling^{1,2}, Haiyang Yu^{1,2}, Kaixin Wang^{1,2}, Mengxin Gai^{1,2}, Yuhang Ma^{1,2} and YongAn Huang^{1,2,*} 

¹ State Key Laboratory of Digital Manufacturing Equipment and Technology, Huazhong University of Science and Technology, Wuhan 430074, People's Republic of China

² Flexible Electronics Research Center, Huazhong University of Science and Technology, Wuhan 430074, People's Republic of China

³ College of Electronic and Optical Engineering & College of Microelectronics, Nanjing University of Posts and Telecommunications, Nanjing 210023, People's Republic of China

E-mail: yahuang@hust.edu.cn

Received 8 March 2022, revised 14 April 2022

Accepted for publication 18 September 2022

Published 14 November 2022



Abstract

Inorganic-based micro light-emitting diodes (microLEDs) offer more fascinating properties and unique demands in next-generation displays. However, the small size of the microLED chip (1–100 μm) makes it extremely challenging for high efficiency and low cost to accurately, selectively, integrate millions of microLED chips. Recent impressive technological advances have overcome the drawbacks of traditional pick-and-place techniques when they were utilized in the assembly of microLED display, including the most broadly recognized laser lift-off technique, contact micro-transfer printing (μTP) technique, laser non-contact μTP technique, and self-assembly technique. Herein, we firstly review the key developments in mass transfer technique and highlight their potential value, covering both the state-of-the-art devices and requirements for mass transfer in the assembly of the ultra-large-area display and virtual reality glasses. We begin with the significant challenges and the brief history of mass transfer technique, and expand that mass transfer technique is composed of two major techniques, namely, the epitaxial Lift-off technique and the pick-and-place technique. The basic concept and transfer effects for each representative epitaxial Lift-off and pick-and-place technique in mass transfer are then overviewed separately. Finally, the potential challenges and future research directions of mass transfer are discussed.

Keywords: mass transfer, microLED displays, transfer printing, interfacial adhesion

⁴ These authors contributed equally to this paper.

* Author to whom any correspondence should be addressed.



Original content from this work may be used under the terms of the [Creative Commons Attribution 4.0 licence](https://creativecommons.org/licenses/by/4.0/). Any further distribution of this work must maintain attribution to the author(s) and the title of the work, journal citation and DOI.

1. Introduction

After liquid crystal display (LCD) and organic light-emitting diode (OLED) display, micro light-emitting diode (microLED) displays are recognized as the next-generation display technology in terms of their superior characteristics, such as ultrahigh brightness ($\sim 10^7$ cd m $^{-2}$, compared with 1500 cd m $^{-2}$ of OLED [1, 2]), nanosecond response time ($\sim 10^4$ and $\sim 10^7$ times shorter than those of OLED and LCD [3], respectively), low power consumption ($\sim 1\%$ of LCD and 40% of OLED [4]), and long lifetime (>10 years, ~ 8 years of LCD, ~ 4 years of OLED [5]), high color reproduction of 140% (75% of LCD and 100% of OLED [6]) and wide view angle (Max. 180° , Max. 89° of LCD and OLED [7]), etc. Currently, many fascinating displays, which cannot be realized with traditional display technologies, become reality with microLED, examples vary from ultra-large displays (e.g. 146 inches ‘The Wall’ developed by Samsung) to ultra-high-resolution (>5000 PPI [8]) virtual reality (VR) glasses and head-up displays. In addition, microLED-based flexible electronics can be served as medical sensors [9–11] to monitor physical/psychological conditions or treat disease [12], and microLED-based visible light communication (VLC) systems with high data rate (≥ 10 Gbps [13–15]) and modulation bandwidth (≥ 100 MHz [16, 17]) make deep-sea communication possible [18, 19]. These excellent features provide a strong incentive to develop high-efficiency and low-cost assembly concepts and processes for large-scale and high-density microLED arrays.

High-resolution microLED displays rely on millions of polychromatic self-emissive elements that consist of red, green and blue (RGB) microLEDs [20]. Figure 1 shows the simplified fabrication process of microLED displays (center part in figure 1) and representative applications that have been described above. Generally, limited by the growth techniques, it is difficult to simultaneously grow RGB microLEDs on a epitaxial wafer (only ~ 8 inches [21, 22]). Thus, deterministic assembly of microLED chips from different growth-donor substrates is required. However, since the feature size of microLED chips are <100 μm , there is a trade-off between tiny feature size and fabrication feasibility. There are three enormous challenges. (a) The extreme transfer efficiency (\sim tens of millions h $^{-1}$) is vital because of their vast numbers. For an 8 K displays, more than ~ 100 million chips need to be transferred onto the receiver substrate, which will take several weeks for traditional pick-and-place techniques (e.g. assembly throughput ~ 8000 chips per hour [23–25] for current flip-chip bonding equipments [23, 26]). (b) The extreme placement accuracy is critical for microscale chips ($\sim 5\%$ of the microLED chip size [20, 27]). For example, the transfer error of a 10 μm -sized microLED chip should be smaller than 0.5 μm , which is far beyond the accuracy of traditional transfer techniques (e.g. only ~ 30 μm [28]). (c) The extreme reliability ($\sim 99.9999\%$ [21]) is also essential. Otherwise, a 0.01% failure rate could result in thousands of dead pixels [29]. In short, traditional assembly methods are not practical for MicroLEDs.

As a revolutionary technique specified by industry and mass transfer, which can release massive microscale chips (e.g. \sim millions h $^{-1}$) from the donor/growth substrate an efficient rate and move them to the backplane/receiving substrate with high precision and reliability, it has proven to be a promising solution. These techniques typically introduce physical/chemical interactions (e.g. Van der Waals (VDW) force [33, 34], fluid tension [35], electrostatic force [36, 37], laser ablation [38, 39], selective etching [40, 41], etc) to switch the adhesion/de-adhesion state of the interface between the donor/transfer medium (e.g. elastomer stamp, fluid) and microLED chips in a highly controlled, scalable, and accurate way. For instance, the micro-transfer printing (μTP) utilized an elastomer stamp with thousands of tiny posts (~ 10800 posts [42]) to control the interface adhesion by tuning the peeling speed. Thus, microscale and even nanoscale structures can be selectively transferred in parallel. X-Celeprint demonstrated that μTP can achieve the transfer reliability (chip size of 8×15 μm^2) of $\sim 99\%$ [43], with the maximum transfer efficiency of >6.5 million h $^{-1}$ [44] and the placement accuracy of ~ 1.5 μm [45]. Recently, different kinds of lasers have been introduced to enable digital and parallel transfer processes with highly enhanced throughput, cost-efficiency, and process flexibility. Especially, extremely high assembly rates (>100 million h $^{-1}$) can be achieved by arrays of laser beams [39, 46]. Because of recent significant progress, these mass transfer techniques could become candidates for industrialized manufacturing of microLED displays.

Recently, many review papers have merely focused on microLED displays [5, 7, 47–49], which mainly concluded the technological path of microLED chips or the solution of full-color displays. Here, we attentively present an in-depth analysis of the latest developments of mass transfer techniques. In section 2, we first discuss the general assembly process (i.e. epitaxial lift-off and pick-and-place process) of microLED displays and highlight key challenges of mass transfer techniques. Then, various state-of-the-art mass transfer strategies and principles adopted in different production steps of microLED displays are described in the subsequent two sections. Finally, we discuss the future opportunities and challenges in this field.

2. Evolution of microLED displays and mass transfer technique

2.1. Basic knowledge of mass transfer

The assembly of microLED chips generally includes several key process steps, including releasing massive microLED chips from the donor/growth substrate (i.e. epitaxial lift-off process), adjusting pitch size, and finally aligning and moving them to a backplane/receiver substrate (i.e. pick-and-place process) [3, 42]. For achieving full-color microLED displays, mass transfer techniques can be divided into two categories [50, 51]. (a) The first strategy is the selective batch

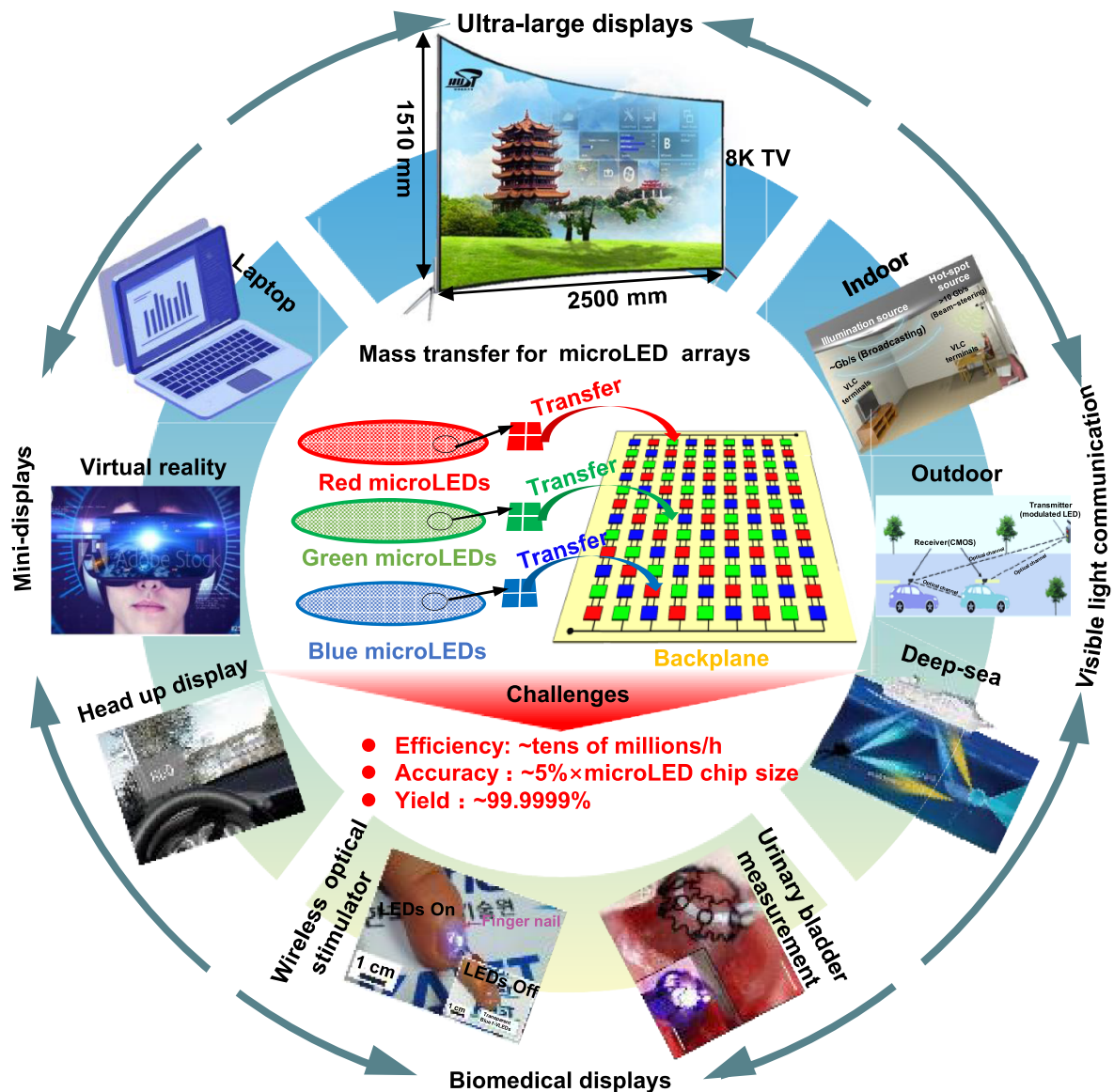


Figure 1. The manufacturing process of microLED displays and representative examples of microLED displays. From [11]. Reprinted with permission from AAAS. [30] John Wiley and Sons. ‘Visible light communication’. [19] John Wiley & Sons. Reprinted by permission from Springer Nature Customer Service Centre GmbH: Springer Nature, Sci. Rep. [31] © 2019. Reproduced from [32]. CC BY 4.0.

transfer of RGB microLED chips, respectively (figure 2(a)) [52]. At the epitaxial lift-off process, microLED chips with different colors are separated from their growth substrates (figures 2(a-ii)). Next, in the pick-and-place process, a transfer medium is used to pick up the RGB microLED chips from different growth substrates (figures 2(a-iii)–(a-v)), followed by a delivery step to place RGB microLED chips to the target receiver substrate (figure 2(a-vi)). (b) The second strategy is the selective batch transfer of monochromatic Blue/UV microLED chips (figures 2(b-ii, iii)), followed by integrating color conversion (figures 2(b-iv, v)) such as ink jet printing of quantum dots (QD [53–55]) or light-emitting polymer [56], as shown in figure 2(b). Notably, only for some special kinds of displays with extremely high resolution (e.g. AR [57, 58]), the entire blue microLED chips can be directly transferred

right after the epitaxial lift-off process (termed as ‘monolithic transfer’ [59–62]) with no need for changing the original distance between adjacent microLED chips [63]. However, the color conversion techniques are still plagued by some technical issues, such as difficulties in heat dissipation, low color conversion efficiency, and thermal stability [2, 64–66]. Therefore, till now, a mass transfer process is still an indispensable step.

Essentially, a mass transfer technique fundamentally relies on the efficient, reliable, and parallel control of interfacial adhesion at some critical interface, i.e. microLEDs/growth substrate, transfer medium/microLEDs, and microLEDs/receiver. Firstly, the epitaxial lift-off process determines the interface adhesion state of the microLEDs/growth substrate. For the fabrication of microLEDs, a buffer/sacrificial layer

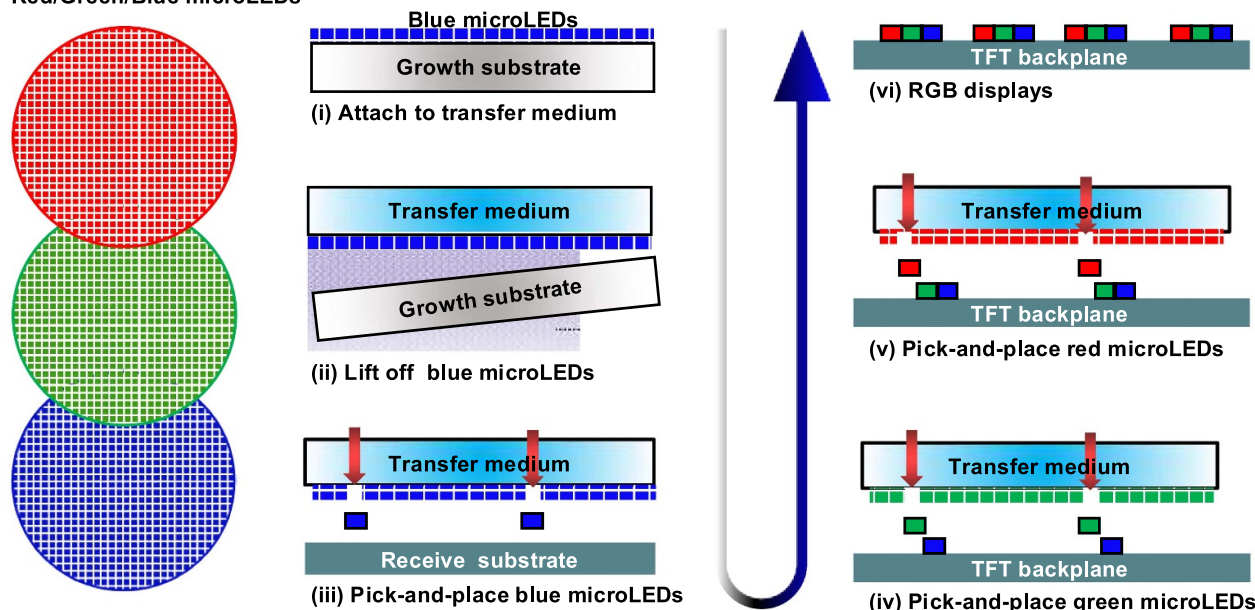
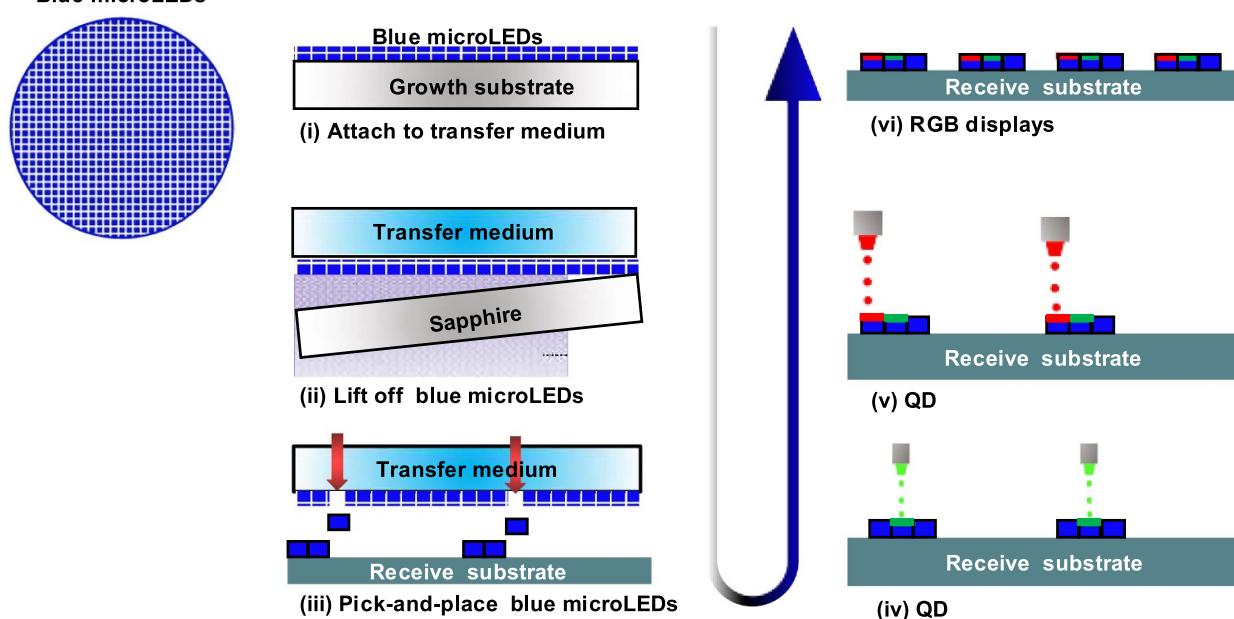
(a) Mass transfer RGB microLEDs**Red/Green/Blue microLEDs****(b) Mass transfer blue microLEDs+QD****Blue microLEDs**

Figure 2. Two general process strategies for fabricating microLED displays. (a) The selective batch transfer of RGB microLED chips respectively. (b) Schematic illustration of the selective batch transfer of monochromatic blue microLEDs, followed by integrating color conversion.

must be introduced on the growth substrate (sapphire) to reduce the effect of lattice/thermal mismatch [67]. The GaN buffer layer connects with the sapphire substrate by strong sp³-type covalent bonds (i.e. chemical interactions, $\sim 1000 \text{ kJ mol}^{-1}$ [41, 68]). This strong adhesion makes it very difficult to regulate interfacial adhesion only by a physical stimulus. Therefore, high-energy processes (e.g. laser [69, 70])

or chemical etching is required [40, 41]. Due to a complicated coupling between the physical (e.g. laser-induced heating and molten, and shock [39]) and chemical (decomposition of the sacrificial layer [71, 72]) processes, mass transfer techniques firstly face a serious challenge of how to control the epitaxial lift-off process selectively and precisely. A wide range of factors, such as the chip thickness [73], structure

[74, 75], size, and the method for injecting energy (laser or etchant) at the interface for peeling, affect the final interface adhesion state, as well as the quality of the peeled chip. Typically, the epitaxial lift-off process can only enable the direct preparation of a limited range of microLED displays, while for large-area displays with variable pixel arrangements, additional pick-and-place processes are required.

By contrast, physical adhesion (e.g. VDW force [76, 77], fluid tension [78–80], electrostatic force) plays a critical role in pick-and-place processes. The ability of the transfer medium to switch adhesion from the strong to the weak state in a highly parallel, efficient, and accurate manner is the main factor to determine the capability of mass transfer techniques. During the pick/retrieval step, the adhesion strength of the transfer medium/microLEDs interface must be stronger than that of the microLEDs/donor, thus, allowing for the successful peeling of microLED chips from the donor substrate. During the place/printing step, a low interface adhesion strength is favorable for the transfer of microLEDs to the receiver substrate. Compared with chemical adhesion, some physical adhesion could provide a much lower and variable adhesion strength [68]. For typical reversible adhesive systems, the critical force for the interface separation F_c is found to be $F_c = \sqrt{G_{\text{crit}}} \sqrt{A/C}$ [81], where G_{crit} (critical energy release rate) is a property set by the materials comprising the interface, A is the surface area of adhering, and C is the system compliance. This relationship suggests that the physical adhesion of an interface is governed by three key parameters, which are dependent on both the geometry and material properties of the interface [82]. Consequently, how to regulate the above three key parameters by external stimulation to enable reversible adhesive, and how to exert external stimulation in a fast, accurate, selective, and massive way are emphasis and core difficulties of mass transfer techniques.

2.2. A brief chronology of the development of mass transfer

Based on different strategies to realize batch control of interfacial adhesion, a series of mass transfer techniques have been developed. A timeline is illustrated in figure 3 to outline the major milestones toward the development of mass transfer. As a prerequisite step of mass transfer, the epitaxial lift-off technique was first developed in 1978 [40, 83, 84], LEDs with AIAs sacrificial layer were selectively etched by HF, i.e. chemical lift-off (CLO) technique. Soon after, the VDW epitaxial lift-off (VWDE) technique and laser lift-off (LLO) technique was developed in 1997 [85–87]. Unlike the CLO technique, the VWDE technique uses a buffer layer of two-dimensional materials to substantially lower the interface adhesion by replacing chemical adhesion with VDW forces [88, 89]. To improve the peeling efficiency and quality, lasers were introduced to enable the decomposition of the sacrificial GaN layer. Afterward, LLO became the mainstream [90–92]. Meanwhile, the capacity of selective peeling microLED chips provide a simpler solution to adapt the specific pixel arrangement density. Hence, selective lift-off techniques were developed recently [93, 94].

Generally, pick-and-place techniques can be classified into three types according to the relative position of the transfer medium and receiving substrate. (a) The contact μ TP technique requires microLED chips directly in contact with the receiving substrate with the assistance of a special stamp, which was first introduced by Rogers *et al* [33, 95]. In 2013, LuxVue proposed a new design concept of the contact μ TP via the electrostatic force [96, 97]. Typical contact μ TP techniques can reach a high transfer yield (>99.99%). However, the low transfer rate is a bottleneck. (b) The laser non-contact μ TP technique, which introduces a laser to separate the selected chip from the stamp by an interfacial thermal mismatch or blister ejection introduced in 2012 [98–101]. Specifically, these techniques need a certain distance between the stamp and the receiver substrate. The laser non-contact μ TP technique can achieve a high transfer rate (~ 100 million h^{-1}), however, with an unacceptable success rate ($\sim 90\%$). (3) The self-assembly technique utilizes fluid (e.g. fluid self-assembly in 2008 [102–104]) as a transfer medium, and generates gravitational, hydrophobic, or hydrophilic forces to identify and localize microLED chips with specific dimensions. The self-assembly technique could also achieve a high transfer rate ($\sim 99.9\%$, ~ 100 million h^{-1} [105]), nevertheless, with special requirements for microLED chips and receiver panels.

The continuous progress of mass transfer significantly promotes the display quality and integration scale of microLED displays, as shown in the right part of figure 3. The development of microLED displays can be generally divided into three stages: integration of monochrome micro-displays, high-cost integration of large-area displays with low PPI (figure 3. Right), and low-cost integration of any size display with high PPI (future). The microLED display was first invented by Jiang's group in 2000 [2], and the transfer technique at this time could only integrate a few arrays of microLED to form a passive matrix (PM) micro-display. A first 10×10 resolution PM microLED display was achieved in 2001 [111], an array of 32×32 in 2002 [114], 64×64 in 2003, 128×96 in 2004, and many more elements were subsequently reported. In 2008, Rogers' group first used the μ TP technique to realize a 16×16 microLED display [111], which laid the foundation for preparing large-area displays. The first large-area display (55-inch LCD) with 6 million microLEDs launched on the market in 2012, which were fabricated using pick-and-place techniques. In 2014, a full-color microLED display with 1700 PPI resolution was fabricated by contact μ TP [115]. To achieve better resolution and brightness, the active matrix(AM)-driving technique had been introduced [38, 116]. In 2019, a 3.3-inch full-color AM microLED display ($324 \mu\text{m} \times 324 \mu\text{m}$ pixel size) was demonstrated by contact μ TP combined with CLO [116]. The most recent large microLED display (~ 16 K) with a dimension of $21 \text{ m} \times 5.5 \text{ m}$ was presented by Sony in 2019. In recent years, the growing presence of new microLED display products has relied on the progress of mass transfer techniques. However, till now, the high price of manufacturing costs has hindered the popularity of microLED displays.

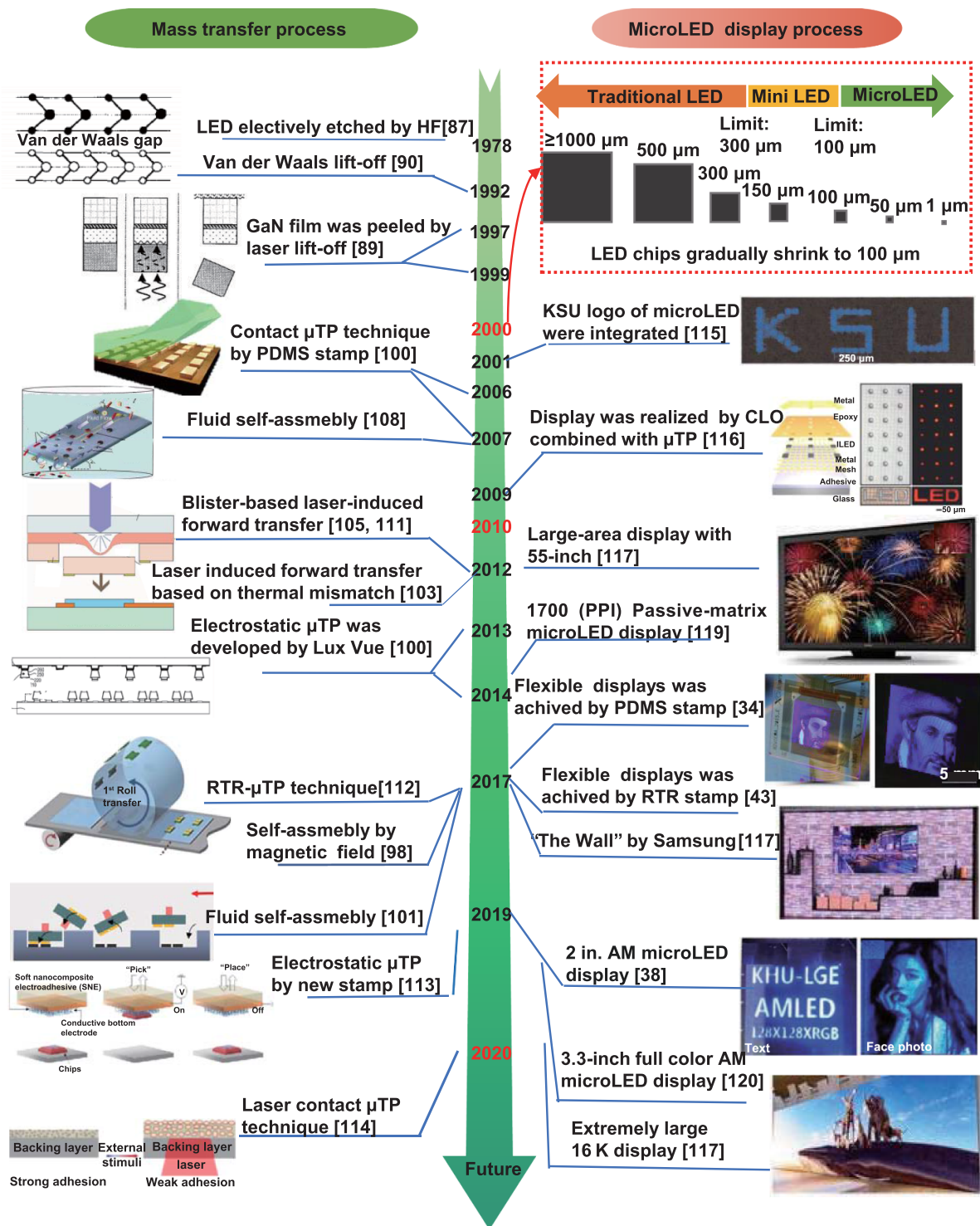


Figure 3. Schematic diagram of a brief chronology of the development of microLED displays and mass transfer techniques. Reprinted from [86], Copyright (1992), with permission from Elsevier. 'GaN film was peeled by laser lift-off' Reprinted [85], with the permission of AIP Publishing. 'Contact μTP technique by PDMS stamp' [33], Reprinted with permission from [106]. Copyright (2007) American Chemical Society. 'Fluid self-assembly', Reproduced with permission from [107]. 'Blister-based laser-induced forward transfer', Reprinted from [108], Copyright (2013), with permission from Elsevier. 'RTR- μTP technique' [109], John Wiley & Sons. 'Electrostatic μTP by new stamp', From [37]. Reprinted with permission from AAAS. 'Laser contact μTP technique', From [110]. Reprinted with permission from AAAS. 'KSU logo of microLED were integrated' Reprinted from [111], with the permission of AIP Publishing. 'Display was realized by CLO combined with μTP ', From [112]. Reprinted with permission from AAAS. 'Large-area display with 55-inch', Reprinted from [113], with the permission of AIP Publishing. 'The Wall' by Samsung, [42] John Wiley & Sons. 'Extremely large 16 K display', [109] John Wiley & Sons. 'Flexible displays was achieved by RTR stamp', Copyright 2017, AIP Publishing. '2 in. AM microLED display' [38], John Wiley and Sons.

Table 1. Comparison of various mass transfer.

Mass transfer	characteristics	Material	Regulating adhesion	Transfer effects (e.g., rate precision and yield)	Advantages	Disadvantages	References
Epitaxial Lift-off (the first step of mass transfer)	Chemical Lift-off	Etching solution	Chemical etching	Low	No thermal stress and shock damage	Low efficiency	[40, 87]
	Laser Lift-off	Excimer Laser Nd:YAG Laser	Ablation	High	Selective peeling whole-area peeling Fast peeling efficiency	thermal stress and shock damage	[38, 132]
	Van der Waals Epitaxy Lift-off	Femtosecond Laser 2D material	Van der Waals force	Low	No thermal stress and impact damage	Small area peeling No selective peeling	[91]
Pick-and-place (the second step of mass transfer)	Contact μ TP	SMP/PDMS/ Magn-etic stamp	Control of van der Waals/ electrostatic/electromagnetic forces at the corresponding interface	Elastomer stamps+ CLO/LLO (~ 10 million h^{-1} , 99.99%, $\pm 1.5 \mu\text{m}$) Roll stamp + CLO/LLO (~ 36 million h^{-1} , 99%/~) Magnetic/ Electrostatic stamp (~ 0.9 million h^{-1})	High transfer precision Selectively transferable	High seal design requirements (e.g. flatness)	[44, 116]
	Laser non-contact μ TP	Excimer Laser Nd:YAG Laser Femtosecond Laser	Gas impact/ blister/thermal mismatch	MPLET+LLO (~ 100 million h^{-1} , $\sim 90\%$, $\pm 1.8 \mu\text{m}$)	Selectively transferable Fast transfer efficiency	Poor transfer accuracy Thermal and shock damage	[106, 111]
	Self-assembly	Fluid media special structure of microLEDs	Complementary chip shapes and fluid forces (e.g., Surface tension)	Fluid assembly + CLO/LLO (~ 100 million h^{-1} , 99.9%)	Parallelizability Transfer	No selective transfer Requires specific chip	[108]
							[112]
							[113]

There is a continuous pursuit of a more cost-effective (relying on extreme high efficiency, yield, and accuracy) mass transfer technique to become the key point of popularity of microLED displays. To facilitate a better understanding of different mass transfer techniques, table 1 summarizes the characteristics, transfer yield, available efficiency, the mechanisms for adjustable interface adhesion, and limitations of all covered techniques. The detailed mechanism of each specific technique will be described in the next section.

3. Epitaxial lift-off technique

3.1. Laser lift-off technique

To achieve the cost-efficient mass transfer process, the epitaxial lift-off process with high yield and reliability is the prerequisite. LLO provides a well-established route for the

epitaxial lift-off process, as shown in figure 4(a) [38, 117, 118]. A laser passes through the transparent sapphire substrate (figure 4(a-ii)), which causes a rapid temperature to rise at the interfacial GaN. The high temperature could make the sacrificial GaN layer decompose into metallic gallium and nitrogen (decomposition temperature $\sim 800^\circ\text{C}$ [73, 119]). As a result, the interfacial adhesion between the sapphire substrate and microLED chips can be largely weakened, and the sapphire substrate can be released by remelting the metal or etching the metal away by HCl (figure 4(a-3)). Various high-power laser sources with photon energy greater than the bandgap of GaN (3.4 eV) have been employed in LLO, such as excimer lasers (248 nm for KrF laser [92, 120], 193 nm for ArF laser [121], and 308 nm for XeCl laser [122]) and Q-switched lasers (355 nm laser [119, 122] and 1064 nm laser which needs additional InGaAsN sacrificial layers [123]) with a short (nanosecond) pulse width.

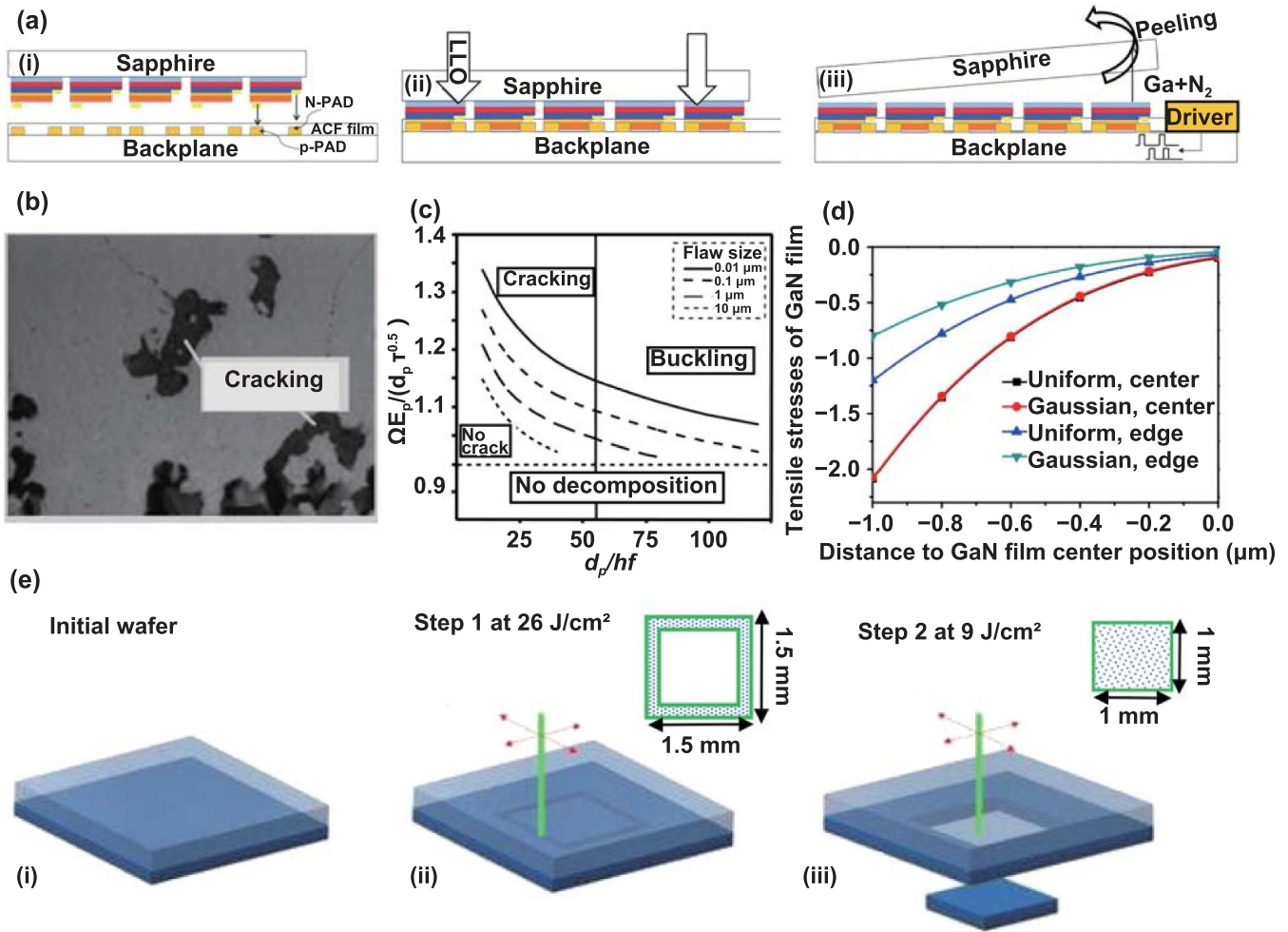


Figure 4. (a) Schematic diagram of the LLO of GaN microLED chips. [38] John Wiley & Sons. (b) Cracking of the GaN film after the LLO process. Reproduced with permission from [73]. Reprinted from [129], Copyright (2003), with permission from Elsevier. (c) The process window of a reliable LLO process is related to several process parameters. Reprinted from [124], with the permission of AIP Publishing. (d) The distribution of tensile stress of GaN film under Gaussian and uniform laser energy distribution. Reprinted from [125], Copyright 2012, with permission from Elsevier. (e) Schematic diagram of the area-selective LLO process. Reproduced from [130]. CC BY 4.0.

A reliable LLO process should not only achieve complete interface separation but also avoid the occurrence of defects that affects the electronic/optical properties of released chips. The adhesion strength between GaN and the sapphire substrate is closely related to the laser energy density, where there exists a threshold for lift-off. Some thermal/mechanical effects (e.g. cracking in figure 4(b) [73], buckling caused by thermal stress, the vapor pressure of nitrogen, thermal shock, etc) of the high-energy laser could make the damage-free lift-off process become a tough challenge. Numerous studies have revealed that it is important to control the laser processing parameters [124]. Typically, as shown in figure 4(c), the process window of the reliable lift-off is related to laser energy (E_p), spot size (d_p), pulse width (τ), and GaN thickness (h_f). Also, compared with the laser spot with uniform distribution of energy density, the laser with Gaussian distribution is better to avoid damage, since the latter can cause a smaller temperature distribution at the edges of the laser irradiated zone, resulting in smaller nitrogen pressure and thermal stress (figure 4(d) [125]). To further improve the process quality,

several optimizations were proposed. Insertion of a sacrificial layer or blocking layer between GaN and sapphire was a popular choice. For example, the carbon nanotube (CNT) was inserted into the GaN-sapphire interface. The CNT could act as a heating wire to elevate the GaN temperature more effectively to reduce the required energy threshold (from 1.5 to 1.3 J cm⁻²). Another attempt is to introduce the femtosecond laser (350 fs–520 nm laser [69, 126]) in consideration of its highly suppressed thermal effect. Especially, the absorption of 520 nm laser relies on two-photon absorption with sub-bandgap excitation [127].

The conventional LLO is a whole-area peeling process, which must rely on additional assembly techniques to accomplish selective integration (to adapt to required pixel arrangement) of heterogeneous RGB microLED chips into the display panel. To remarkably reduce the difficulties in the following assemble process, selective LLO (SLLO) was developed to enhance the overall efficiency of mass transfer [93, 94, 128]. In SLLO, a laser is irradiated to selectively separate microLED chips from sapphire. Generally, controlled adhesion between

Table 2. Representative materials and processes of sacrificial layers.

Active device layer	Sacrificial layer	Substrate	Etch solution	References
GaN	CrN	Sapphire	$\text{Ce}(\text{NH}_4)_2(\text{NO}_3)_6 + \text{HClO}_4$	[133, 134]
GaN	Nb ₂ N	SiC	XeF ₂	[135]
GaN	ZnO	Sapphire	HCL	[136, 137]
GaAs	AlAs	GaAs	HF/NH ₄ OH:H ₂ O ₂ :H ₂ O	[138]
GaAs	Ga ₂ O ₃	Sapphire	HF	[139]
Si{111}	Si	Si	KOH	[140]
GaN	InGaN	Sapphire	KOH	[141]
GaN	AlInN	Sapphire	Nitritotriacetic	[142]
GaN	GaAs	Al _{0.96} Ga _{0.04} As	HF	[4]
GaAs/InGaP	GaAs	GaAs	HCL	[67, 131]

the selected LED and the substrate is key for SLLO. Thus, a lot of studies seek to understand the fundamental relationship between adhesion and laser parameters. Interestingly, figure 4(e) shows a novel SLLO process by a two-step procedure [128]. During the first step (figure 4(e-ii)), the perimeter of the selected area for separation is scanned by a high energy ($\sim 26 \text{ J cm}^{-2}$) femtosecond laser for obtaining high-quality boundaries through laser-induced cracking. In the second step, to avoid chip damage, lower pulse energy ($\sim 9 \text{ J cm}^{-2}$) is used to peel the selected region (figure 4(e-iii)). The experimental results show that this SLLO is capable to fabricate freestanding InGaN/GaN LED chips with thicknesses lower than $5 \mu\text{m}$. Till now, SLLO is still in the early stages and its practical effect needs to be further verified.

3.2. Chemical lift-off technique

Unlike the LLO technique, microLED chips will not undergo any physical/thermal impact during the CLO process, which removes microLED chips by selective wet etching of sacrificial layer between the device layer and sapphire substrate. Table 2 lists some commonly used sacrificial materials for CLO. A typical choice is Si sacrificial layer. Once the Si sacrificial layer reacts with the KOH solution, it will decompose into K_2SiO_3 and H_2 , causing the interface separation. Another example is the AlInP sacrificial layer, which can react with HCL to produce reaction byproducts, AlCl_3 , InCl_3 , PH_3 [67, 131], and after selective etching and epitaxial release, atomically smooth GaAs surfaces. Meanwhile, to avoid the floating away of microLED chips, protective anchors that will not be etched are made together with microLED chips [132], thus allowing the suspension of microLED chips after etching. And then, once the transfer stamp touches the microLED chips to exert some pressure, the anchor will be broken to fully release to the chip.

The relatively low production efficiency is the main problem for CLO since the wet etching of a sacrificial layer often takes several hours [20, 143, 144]. For example, a 2-inch GaN film with a SiO_2 sacrificial layer needs $\sim 56 \text{ h}$ to achieve 70% peeling area by HF etching [145]. To improve the peeling efficiency, sacrificial layers with nanopores [146, 147], nanorods [148], and other special structures (e.g. triangular-shaped hole structure [145], hexagonal-shaped air-void structure [75]) have been developed. Zhang *et al* introduced GaN nanorods

structure by electrochemical etching [74], $\sim 1 \text{ cm}^2$ freestanding GaN layers (thickness ranging from 500 nm to several microns) can be delaminated in $< 20 \text{ min}$. Similarly, for the LED structure with triangular-shaped voids at the GaN/sapphire interface, the peeling efficiency and success rate can be increased 2 and 1.3 times, respectively, compared with the original structures. In addition to these special structural designs, the peeling process can be facilitated by introducing additional electric fields or optical fields (i.e. photoelectrochemical/electroCLO technique). UV illumination is used to generate electron-hole pairs on the semiconductor surface, which can enhance the oxidation and reduction reactions in electrochemical cells. Youtsey *et al* demonstrated that a 4-inch wafer-scale GaN epitaxial material can be peeled off in $< 2 \text{ h}$. Although significant progress has been achieved in CLO, the peeling efficiency and success rate still need further improvements. In addition, how to achieve selective peeling is still a tough challenge for CLO.

3.3. Van der Waals epitaxy lift-off technique

As the latest lift-off technique, the VWDE utilizes 2D materials as the sacrificial layer [89, 149, 150], such as graphene [1], boron nitride (BN) [151, 152], and MoS_2 . There are two significant advantages of this technique. Firstly, 2D materials can overcome the thermal expansion mismatch and in-plane lattice constant mismatch (only $\sim 0.58\%$ [153, 154]) between the GaN layer and growth substrate. Secondly, the VDW force between two adjacent layers of 2D materials is much weaker than the chemical interactions of covalent bonds. Therefore, the VWDE can enable a mechanical lift-off process without the assistance of additional chemical solution or laser, as shown in figure 5(a) [87]. Taking the BN sacrificial layer as an example, figure 5(b) shows a detailed process of the interface separation [155]. After applying mechanical loading, the detaching position is always inside the III-nitride epilayer (at the h-BN/h-BN interface), mainly due to the almost free-sliding path between hBN/hBN. The energy barrier required to separate the hBN/hBN interface (2.0 meV per atom) is lower than that of the GaN/BN interface (4.5 meV per atom). Therefore, the success of VWDE requires precise control of the layer-to-layer bond strength (i.e. 2D/2D layer) between multilayered structures.

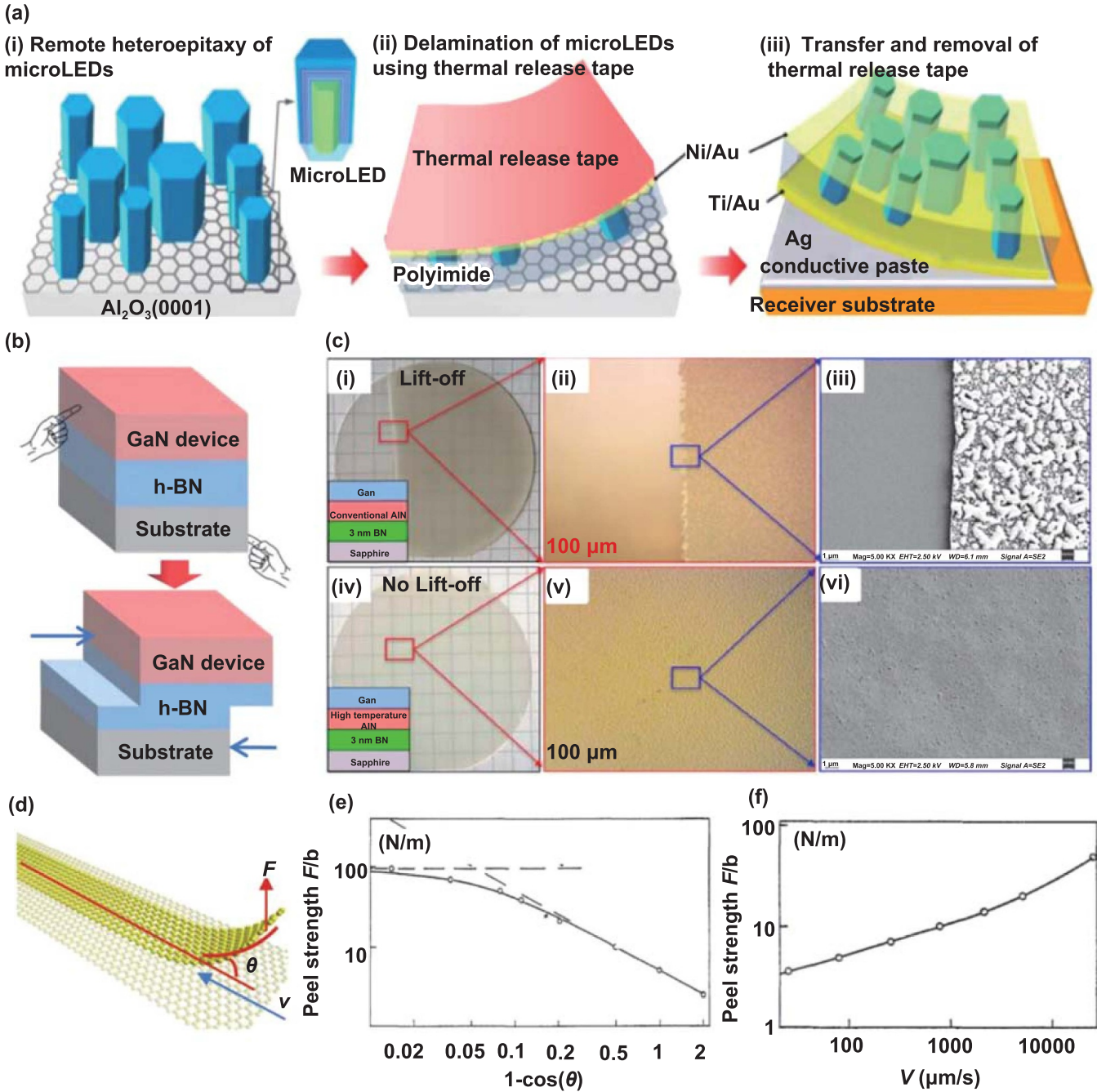


Figure 5. (a) Schematic diagrams of the Van der Waals epitaxy lift-off process. Reprinted from [87], Copyright (2021), with permission from Elsevier. (b) Schematic diagram of the interface separation of the NB release layer. Reprinted from [160], with the permission of AIP Publishing. (c) Photograph, optical microscope, and SEM of GaN/conventional AlN/h-BN (i), (iii) and GaN/high-temperature AlN/h-BN (iv)–(vi) grown on sapphire, respectively. Reprinted with permission from [156]. Copyright (2020) American Chemical Society. (d) A theoretical model of the Van der Waals epitaxy lift-off process describes that the peel strength changes with different peeling angles (e) and peeling speeds (f). (e) Reproduced from [157]. © IOP Publishing Ltd. All rights reserved. (f) Reprinted from [161], Copyright (2021), with permission from Elsevier.

To enable a reliable VDWE, it is essential to fabricate a high-quality GaN layer on a 2D-materials-covered sapphire substrate with controllable interface adhesion. For example, a unique approach of controlling the adhesion of h-BN has been reported by Vuong *et al.*, which could achieve both desired lift-off layered h-BN and mechanically inseparable robust h-BN layers [156]. As shown in figure 5(c), the

quality of AlN/h-BN structures grown at different temperatures (1100 °C and 1200 °C) is compared through optical and scanning electron microscope (SEM) observations. The conventional GaN/AlN/h-BN structure (1100 °C) enables an easy mechanical lift-off process from the growth substrate by using a transparent tape (figures 5(c-i)–(c-iii)), while the GaN/AlN(high-temperature)/h-BN structure was

mechanically inseparable (figures 5(c-iv)–(c-vi)). A possible explanation is that the high-growth temperature leads to Al diffusion into h-BN, which enhances the surface and interface dangling bonds and anchors the layered h-BN. Also, a series of theoretical models (figure 5(d)) indicate that the peeling stress (F), peeling angle (θ), peeling speed (v), and geometric dimension (length and width) of the 2D layer also play important roles in VDWE [157]. Figures 5(e) and (f) present the peel strength change with different peeling angles and peeling speed. The peel strength increases linearly with the peeling speed while decreasing with the peeling angle. Therefore, a large peeling speed with a small peeling angle could be more appropriate for VDWE.

Although substantial progress has been made in VDWE in recent years, there is still a lot of studies that need to be done before mass production. One of the studies is to ensure the film quality of GaN. Especially, the lack of dangling bonds on the surface of 2D materials makes it difficult to ensure nucleation, thus further optimization schemes need to be introduced, such as the introduction of buffer layers (e.g. aluminum buffer layers, whose aluminum is more easily bonded to BN [158]) or nanopatterned sapphire [159]. Meanwhile, area-selective lift-off with large areas is still rarely studied. The need to consider, for example, the effect of inhomogeneities in large-area 2D materials due to local buckling or defects on the VDWE process still needs further study. Finally, further exploration of inexpensive techniques to prepare 2d materials is needed.

4. Pick and place technique

4.1. Contact μ TP technique

As the most common form of pick and place, contact μ TP generally utilizes a specially designed stamp as a medium to enable the batch transfer of microchips between the donor substrate and the receiver substrate. At the beginning, a proper preload is applied on the stamp to ensure full contact between the stamp and chips, which should provide enough adhesion to pick up chips from the donor substrate. Then, the stamp is brought into contact with the receiver substrate by precise manipulation of the stamp/chip adhesion to print chips onto the receiver substrate. The whole pick-and-place process is highly demanded in a selective and massively parallel way for high throughput. Thus, the key to successful contact μ TP is a timely, flexible and ingenious use of adhesion modulation of the stamp/ink interface. According to the control principle of interfacial adhesion, the contact μ TP techniques can be classified as follows: (a) VDW contact μ TP technique; (b) Electrostatic/Electromagnetic contact μ TP technique.

4.1.1. Van der Waals contact μ TP technique. VDW contact μ TP technique utilizes a viscoelastic stamp (e.g. PDMS) to introduce VDW adhesion force. By cleverly manipulating the interface adhesion (denoted as the critical energy release rate G_{crit} for peeling), several advanced transfer printing techniques have been developed. In figure 6(a), Rogers's group verified that the adhesion strength of a viscoelastic stamp

is rate-dependent [106, 162, 163]. The result shows that the adhesion switching ratio (the achievable maximum adhesion strength for high peeling rate divided by the minimum adhesion strength for low peeling rate) is over 3. Based on this adhesion switching ability, as shown in figure 6(b), microLED chips can be separated from the growth substrate with a quick peeling step and printed on the receiver with a much slower peeling process [164]. A higher adhesion switching ratio is directly related to the success rate for contact μ TP. RTR contact μ TP with a ~ 100 adhesion switching ratio was developed by KIMM (figure 6(c)) [109]. The results revealed that the adhesion of the RTR stamp is not only related to the peeling rate but also determined by the geometry dimension and moving direction of angled posts of the stamp. Figures 6(d) and (e) show the predicted interface adhesion (G) with the rolling speed for different rotation directions and roll radius R . A much higher G can be achieved by forward rolling with a large R . Thus, forward rolling is suitable for separating microLED chips from the growth substrate with an appropriate roll radius. Generally, for the selective batch transfer of microLED chips with specific arrangements and sizes, special PDMS stamps were designed and fabricated with structured micro-pillars. So far, these special PDMS stamps with structured micro-pillars can be fabricated by nanoimprint lithography [165–167], laser ablation [168, 169], soft lithography [95, 170, 171], or silicon-based mold fabrication [172, 173], when covering a small area. However, it is difficult to maintain the high uniformity of the micro-pillars over large areas. Also, the clustering [174–176], self-collapse [177, 178], and other phenomena of adjacent micro-pillars during the contact μ TP process need to be strictly avoided, which still causes many difficulties.

To enable the substantial control of the interface adhesion for an enhanced transfer success rate, several improvements of VDW contact μ TP have been proposed by modifying the contact area or elastic modulus of the stamp, such as the surface-relief-structured stamp with a ~ 1000 adhesion switching ratio [95], and an inflatable stamp with a ~ 50 adhesion switching ratio [181], etc. These improvements have been well summarized in some other reviews [77, 182, 183, 190]. In addition to the improvement of the adhesion switching ratio, another attempt is to enhance the efficiency and flexibility of the transfer process by incorporating lasers in contact μ TP, namely laser-assisted contact μ TP [39, 98, 184, 186]. The selective transfer can be easily obtained by controlling the shape of the laser spot, as well as the scanning paths, which can avoid the use of the above-mentioned sophisticated stamps with microstructures.

Figure 7 shows several representative laser-assisted contact μ TP techniques. Huang *et al* have demonstrated that reversible VDW adhesion can be achieved by utilizing the shape memory (SMP) stamp with pyramid posts, as schematically described in figure 7(a) [184]. At first, an SMP stamp with pyramid posts is heated and pressed onto the target chip for achieving a large contact area, then its shape is fixed by cooling (figure 7(a-i)). Subsequently, the chip was peeled from the growth substrate due to the high adhesion (figure 7(a-ii)). For the printing step (figure 7(a-iii)), a laser heats the SMP to initiate shape recovery to largely reduce the contact area,

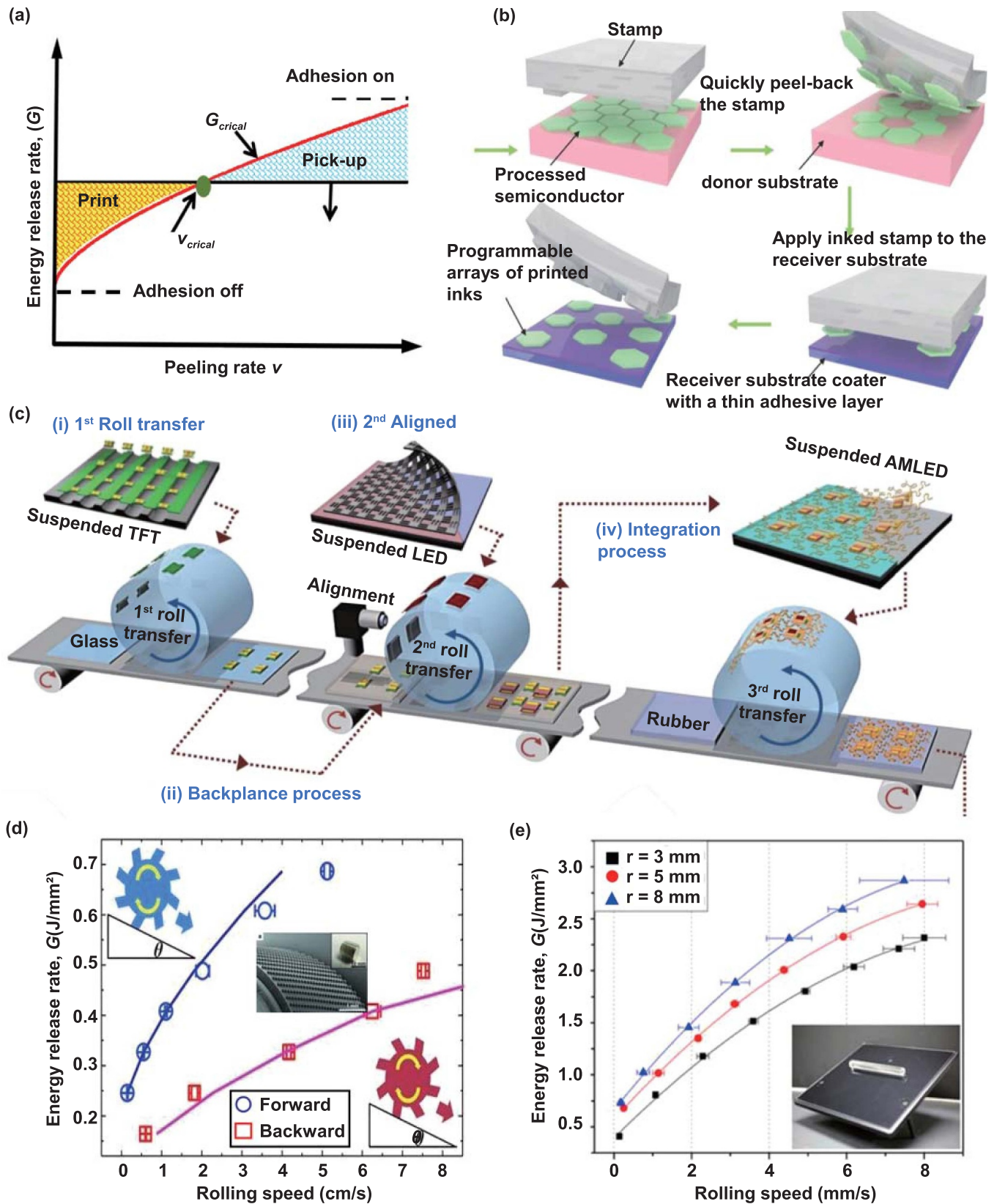


Figure 6. (a) Schematic illustration of the relationship between the critical energy release rate G and peeling rate. Reprinted with permission from [106]. Copyright (2007) American Chemical Society. (b) Schematic illustration of the kinetically-controlled μ TP technique process. [164] John Wiley & Sons. (c) Schematic illustration of the RTR contact μ TP process. [109] John Wiley and Sons. (d) Demonstrations of rotation direction-dependent adhesion of an angled post roller. [179] John Wiley and Sons. (e) Demonstrations of radius-dependent adhesion of an angled post roller. Reprinted with permission from [180]. Copyright (2016) American Chemical Society.

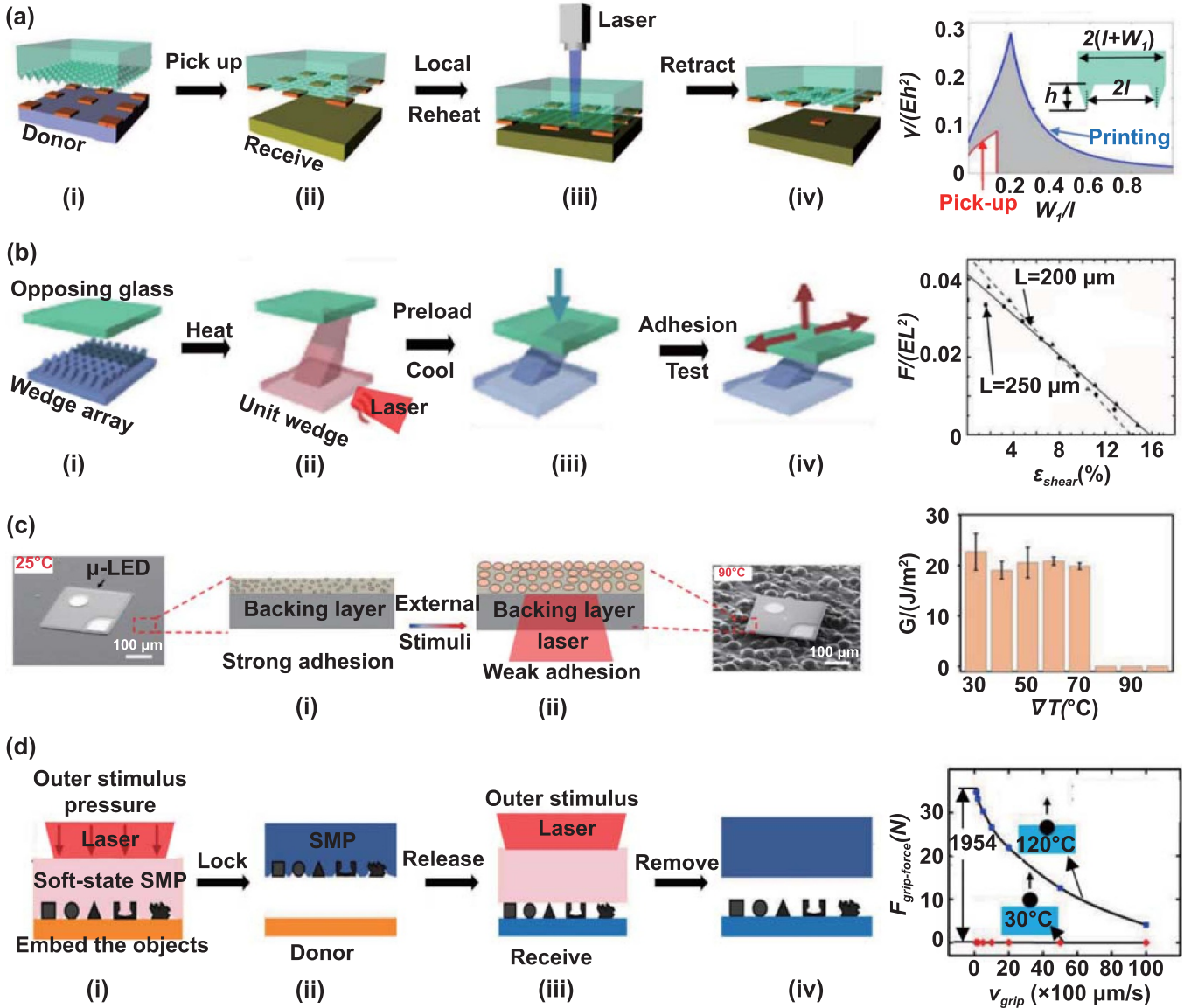


Figure 7. (a) Programmable transfer printing process via a shape memory stamp with trapezoidal posts (left). Valid trapezoidal post designs in terms of W_1/l and $\gamma l/Eh_0$ to achieve successful μTP with the pickup and printing (right), and the top right panel shows the structural dimensions of the trapezoidal post. Reprinted with permission from [184]. Copyright (2016) American Chemical Society. Reprinted from [185], Copyright (2015), with permission from Elsevier. (b) Schematic illustration of a laser-assisted μTP process via shape memory stamp with vertical posts (left). Theoretical and experimental results of the functional relation between normalized pull-off force $F/E_{stamp}L_{post}^2$ and the shear strain ϵ_{shear} , for the post width $L = 200 \mu m$ and $L = 250 \mu m$. Reprinted from [187], Copyright (2016), with permission from Elsevier. Reprinted from [188], Copyright (2012), with permission from Elsevier. (c) Schematic illustration of a laser-assisted μTP via a gripper stamp process (left), the top right panel shows energy release rate (G) of stamp after being heated on a hotplate at various temperatures. From [110]. Reprinted with permission from AAAS. (d) Schematic illustration of the gripping and release process of the shape memory gripper (right). Experimental results of the functional relation between grip strength $F_{grip-force}$ and grip speed at temperatures of $120^\circ C$ and $30^\circ C$. From [189]. Reprinted with permission from AAAS.

thus, the chip could be successfully transferred (figure 7(a-iv)). Theoretical analyses (figure 7(a), right) show that the regions of successful transfer printing are determined by the dimensionless constant W_1/l and $\gamma l/Eh_0$, where W_1 , l , h_0 are the spacing, height, and length of the trapezoidal posts, E is the elastic modulus of the stamp, and γ is the work of adhesion [189]. Therefore, a rational design of the pyramidal post is required. The pyramid posts could be further replaced by vertical posts (figure 7(b), left [185]). The lateral displacement

of a vertical post was induced by laser heating, which causes a mixed-mode loading at the interface for decreasing adhesion (figure 7(b-iii)). Similarly, a fracture mechanics model is developed to calculate the pull-off force (in figure 7(b), right). The pull-off force F decreases with the shear strain ϵ_{strain} , and it can be predicted by the scaling law: $\frac{F}{E_{stamp}L_{post}^2} \approx \left(\frac{24}{\pi E_{stamp}L_{post}}\right)^{0.5} - \frac{1.3\epsilon_{strain}}{L_{post}}$, where Γ_0 is fracture toughness of the stamp/micro-device interface [187], E_{stamp} and L_{post} are the

stamp elastic modulus, post width, and post height, respectively. More recently, Wang *et al* invented a simple shape-conformal stamp with micro-spheres [110]. In the pick-up process, due to the strong viscosity of the shape-conformal stamp, the device is peeled off from the donor substrate. In the printing process, the extremely large volume expansion of micro-spheres (figure 7(c-ii)) can rapidly induce hierarchical microstructures on the surface of the adhesive layer and decrease the energy release rate markedly by heating (figure 7(c), right), and the adhesion can be manipulated in the range of ~ 100 times of magnitude. To massively assemble the objects with a wide range of scales, shapes, and quantities, a universal SMP block has been invented (figure 7(d) [188]). Since the stiffness of the SMP can reversibly change ~ 1000 times under laser stimulus, objects can be embedded in the SMP under pressure and grasped (figure 7(d-i)). Then, the shape recovery upon the stimulation of a laser could facilitate the releasing process (figure 7(d-iii)). The adhesion could be reduced in three orders of magnitude (figure 7(d), Right).

Despite these achievements in laser-assisted contact μ TP, there are still some bottlenecks that need to be addressed. Typically, the laser-induced adhesion switch mostly is a thermal activation process, however, the absorption of the laser still relies on the surface of the chip. The challenge is how to effectively avoid possible thermal damage on chips. An improved method is to add some laser absorbing material on the stamp surface, such as carbon black particles for absorbing 808 nm laser [191, 192]. Moreover, little research has investigated the actual transfer efficiency and reliability of laser-assisted contact μ TP techniques.

4.1.2. Electrostatic/electromagnetic contact μ TP technique.

Electrostatic/magnetic contact μ TP techniques utilize some special stamps that can generate switchable electric/magnetic force. Representatively, as shown in figure 8(a) [37], a ground-breaking electrostatic stamp was developed by Hart *et al*, which is composed of soft nanocomposite electroadhesive (SNE, multi-walled Al_2O_3 -coated CNTs, diameter of ~ 20 nm) with a conductive bottom electrode (titanium nitride, TiN). When an appropriate voltage (>100 V) is applied, the strong electrostatic adhesion force of the SNE stamp can overcome the adhesion between the target chip and donor substrate (figure 8(a-ii)) for picking up. Since the intrinsic dry adhesion of SNE is very low, turning off the voltage allows the easy release of the object at the desired location (figure 8(a-iii)). As shown in figures 8(b) and (c), the external voltage, CNT fiber density, and Al_2O_3 thickness are the major factors that affect the electrostatic adhesion of the SNE stamp. The adhesion switching ratio increases with the external voltage, and CNT density decreases with the Al_2O_3 thickness. Therefore, with a proper design of the SNE stamp, this electrostatic contact μ TP technique could pick up objects with sizes of ~ 20 nm to $100 \mu\text{m}$.

Compared to the electrostatic contact μ TP technique, the electromagnetic contact μ TP technique requires the microLED chips with an additional magnetically sensitive

layer to generate magnetic force [193, 194]. The electrostatic/electromagnetic contact μ TP technique envisions a promising approach for the integration of extremely small objects. However, the mass transfer of tiny chips with predefined patterns remains a significant challenge, which fundamentally relies on the preparation and patterning of the stamp. As shown in figures 8(d) and (e), the above-mentioned SNE stamps ($\sim 100 \mu\text{m}$ long) can be patterned by CVD, chemical vapor deposition methods [195–197]. However, the large-area preparation of CNT arrays is still in a preliminary stage, with typically reported preparation abilities of only $\sim 200 \text{ g h}^{-1}$ and an area of $\sim 300 \text{ mm}^2$. Meanwhile, the cyclical stability, the influence of the charge accumulation, and the homogeneity of magnetic material (for the electromagnetic contact μ TP) require further verification.

4.2. Laser non-contact μ TP technique

For a non-contact μ TP process, the stamp does not directly contact the receiver substrate. Thus, the success of the placing process is independent of the topography and properties of the receiving surface. Without the assistance of the receiver substrate, the stamp should achieve infinite adhesion switchability to launch the selected chip away from the stamp. The laser-driven non-contact μ TP is the only technique that can be manipulated in a non-contact transfer mode reported so far, resulting from the remotely injected energy (laser) at the chip/stamp interface. Generally, for a laser non-contact μ TP process, a shaped laser irradiates through a transparent substrate, bringing about physical changes or chemical reactions at the interface, such as local deformation, vaporization, and thermal stress mismatch, to achieve the switch-off of the chip/stamp adhesion. Therefore, a selective transfer process with local, non-contact outer stimuli (laser) could greatly enhance the versatility of mass transfer techniques. The most significant advantage of laser non-contact μ TP is the scalable chip size, shape, transfer frequency, and selective/parallel mode, which are mainly determined by the laser beam that can be flexibly controlled by the setup of laser equipment and optics. In this section, three types of laser non-contact μ TP techniques are reviewed.

4.2.1. Laser-induced forward transfer (LIFT). LIFT is a major kind of laser-assisted printing technique allowing the deposition of a wide range of functional materials/structures into user-defined patterns. Figure 9(a) illustrates a typical LIFT process including five main components [198–201]: a laser pulse, a stamp with a transparent substrate, and a laser absorbing layer (dynamic release layer, DRL), a target chip, and a receiving substrate [199, 202]. A laser passes through the transparent substrate and is absorbed by the DRL, leading to a fast increase in the interfacial pressure due to the ablation or vaporization of the DRL. The high pressure will push the chip from the donor to the receiver. The common choices of DRLs are triazene polymer (TP) and metal films (Ti, Au, and Pt) with a thickness of hundreds of nanometers. In particular, TP is a

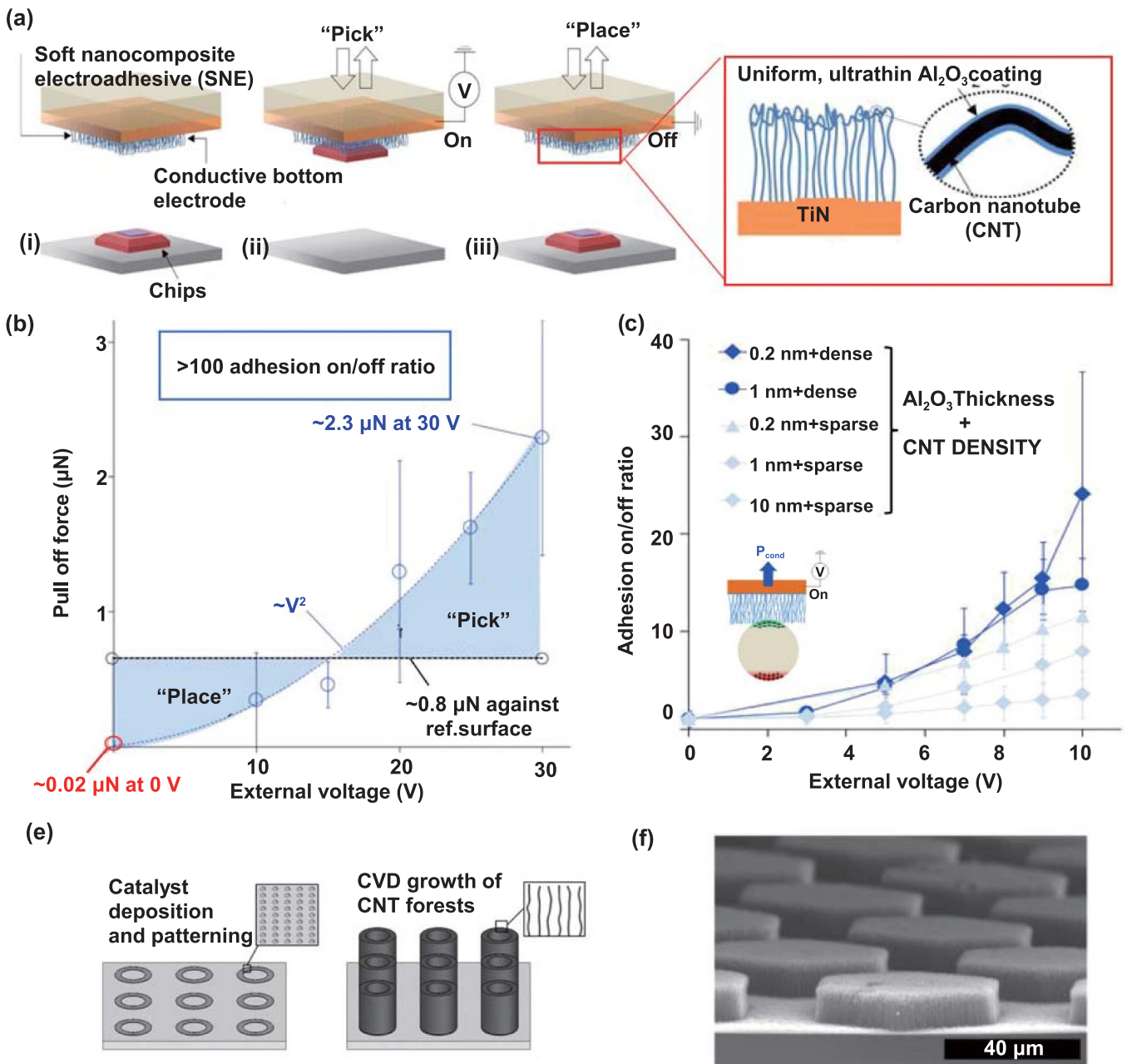


Figure 8. (a) Schematic illustration of a pick-and-place procedure via an SNE stamp. (b) The relationship between the external voltage and the electrostatic adhesion force. (c) Adhesion on/off ratio of Al_2O_3 -CNT SNE with different Al_2O_3 coating thicknesses (approximately 0.2, 1, and 10 nm) and different fiber densities (sparse and dense). From [37]. Reprinted with permission from AAAS. (d) Patterned CNTs made by chemical vapor deposition. [196] John Wiley and Sons. (e) An SEM image of patterned CNTs. [197] John Wiley and Sons.

kind of polymer that contains aryl-triazene chromophores with high absorption at UV wavelength. It can be decomposed at very low laser fluence (only $\sim 50 \text{ mJ cm}^{-2}$ [203, 204]), thus making it easier to enable the transfer process and reduce the risk of thermal damage.

However, there are still some considerable performance bottlenecks of LIFT that will bring tough difficulties to mass transfer. One challenge is the generation of shock waves during the LIFT process. As shown in figure 9(b), by time-resolved shadowgraph, the shock wave is found to be faster

than the chip, which will be reflected by the receiver and interact with the flying chip [205, 206]. This interaction could cause unwanted deflection of the chip orientation, as well as chip damage. Optimization of some key process parameters, such as the laser energy, the gap between receiving substrate and stamp, the DRL thickness, and environmental pressure has been tried to avoid the impact of shock waves. Shaw-Stewart *et al* revealed that the intensity of the shock wave decreases with the gap distance ($<0.5 \text{ mm}$) at normal atmospheric pressure, so it is possible to eliminate the shock wave by choosing

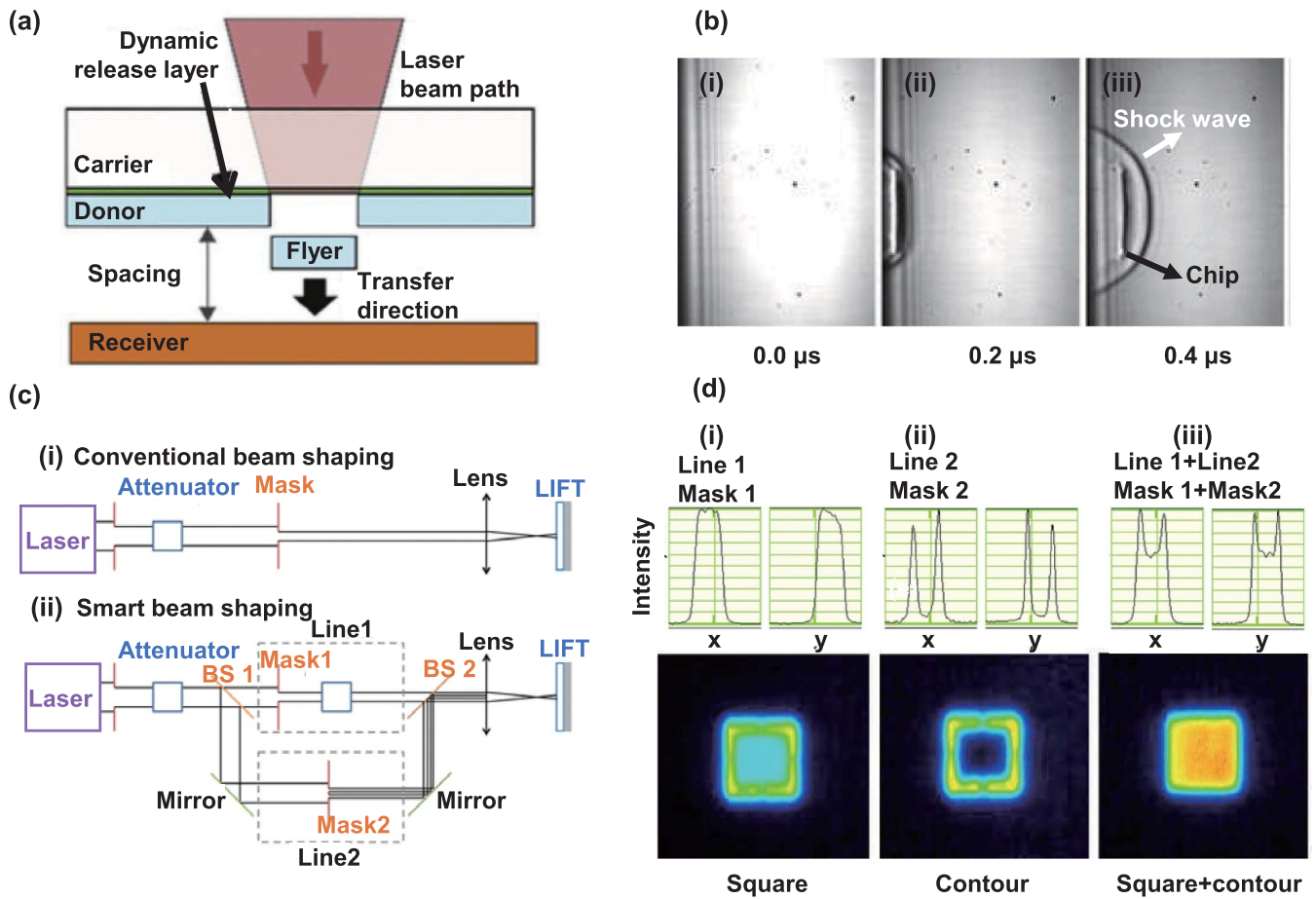


Figure 9. (a) Schematic illustration of laser-induced forward transfer process. Reprinted from [208], Copyright (2017), with permission from Elsevier. (b) Detailed illustration of shock wave and chip drop status diagram: (i) Laser radiation in the dynamic release layer; (ii) Ablation of the dynamic release layer; (iii) Shockwave generation and chip transfer. Reprinted from [206]. Copyright (2010) American Chemical Society. (c) Schematic of the laser-induced forward transfer experimental setups: (i) A conventional shaping setup, and (ii) smart beam shaping setup using a double mask system. (d) Beam profiles with associated intensities in x and y shaping setup: (i) Beam profile of line 1 (square); (ii) Beam profile of line 2 (contour); (iii) Beam profile of line 1 and 2 (square & contour). Reprinted from [209], Copyright 2015, with permission from Elsevier.

a larger gap (~ 1 mm [207]). Also, the environmental pressure can be regulated, such as less than 100 mbar or in a vacuum, to enable a safe transfer in a gap distance of less than $20 \mu\text{m}$.

Another challenge is how to achieve the non-destructive transfer of ultrathin chips. Even in a vacuum, although there is no air resistance and shock waves, it is still difficult to ensure the safety of the chip due to the extremely high impact velocity ($\sim 1200 \text{ m s}^{-1}$ [206]). Lower laser energy certainly can result in a smaller impact speed [206], thus, some specific strategies have been developed, including reducing the DRL thickness and introducing smart intelligent spot systems [210]. Rapp *et al* proposed an intelligent beam shaping (SBS), as shown in figure 9(c-ii) [210]. Different from a conventional LIFT beam system (CB, line 1, figure 9(c-i)), SBS requires another mask system, i.e. a second line (Line 2) on Line 1. Line 2 is created by using a beam splitter before Mask 1 so that the laser beam passes through the second mask (Mask 2). In addition, an additional energy attenuator is placed after Mask 1 (Line 1) to reduce the energy in the center of the spot. The resulting irradiation on the stamp is the combination of Masks 1 and 2, as

presented in figure 9(d-iii). This setup allows for higher energy at the edge of the spot (figure 9(d-ii)) while maintaining a lower and more uniform energy distribution in the central area (figure 9(d-i)). Due to this specially designed energy distribution, only the laser energy at the edge (Line 2) is required to reach the transfer threshold, while allowing the center energy (Line 1) to be reduced to half of the transfer threshold, thus reducing damage. Although lots of achievements were made in LIFT, it still needs to be further improved to form a stable process window.

4.2.2. Blister-based laser-induced forward transfer technique.

To fundamentally avoid the impact of shock waves and minimize the risk of chip damage, a blister-based laser-induced forward transfer technique (BB-LIFT) was developed [211–213]. Unlike the traditional LIFT, BB-LIFT utilizes a double-layered stamp that is composed of a DRL (e.g. $15 \mu\text{m}$ thick polyimide [100, 214] or $80 \mu\text{m}$ thick aluminum [215, 216]) and an adhesive layer (e.g. $70 \mu\text{m}$ thick

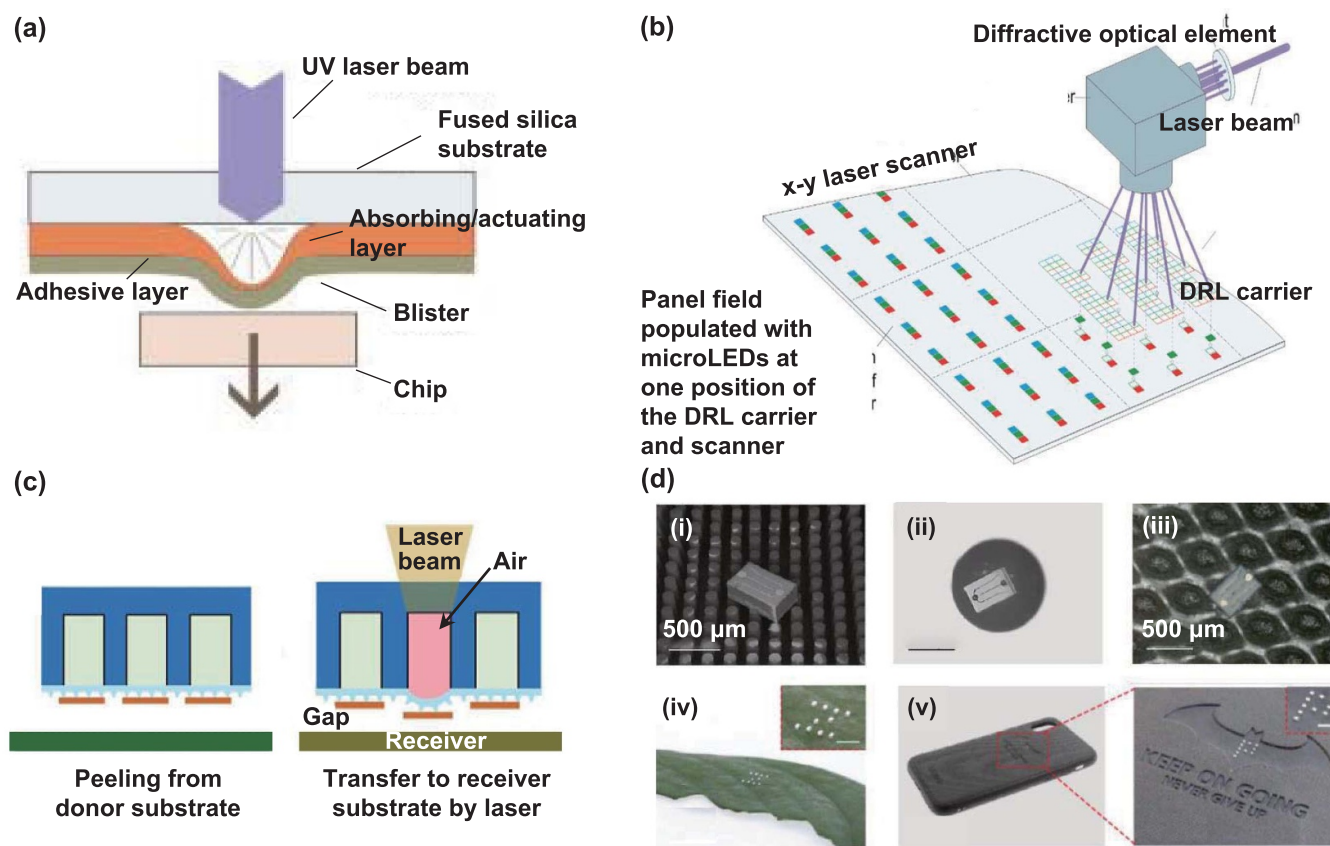


Figure 10. (a) Schematic illustration of the principles of blister-based laser-induced forward transfer. Reprinted from [108], Copyright (2013), with permission from Elsevier. (b) A schematic illustrating the MPLET concept [101]. [46] John Wiley & Sons. Copyright 2018, WILEY-VCH. (c) Schematic illustration of the principles of reusable blister-based laser-induced forward transfer process. (d) Presentation of microLED chips ($400 \times 200 \times 90 \mu\text{m}$) printed onto various planar and curvilinear surfaces: (I) A PDMS pillar array with a pillar diameter of $100 \mu\text{m}$; (II) Steel sphere with a diameter of 1 mm ; (III) A piece of paper; (iv) A Scindapsus leaf to form a letter 'Z'. (v) A mobile-phone shell to form a letter 'P'. (c), (d) Reprinted by permission from Springer Nature Customer Service Centre GmbH: Springer Nature, Nat. Commun. [217], © 2018.

PDMS [216, 217]) to bond chips. During laser irradiation, only a small portion of the DRL is ablated to provide impact energy via gas products. The DRL can encapsulate the shock wave inside by creating an expanding blister that serves as a soft ejector to push the chip more gently toward the receiving substrate, as shown in figure 10(a) [108]. Thus, instead of directly using the impact energy of the ablated DRL, the created blister can also realize a quick release (the transfer process takes $<50 \mu\text{s}$) with higher accuracy (reported minimum placement error of $1.8 \mu\text{m}$) and less damage. Moreover, the most significant advantage of BB-LIFT is high scalability. Parallel laser-enabled transfer (MPLET) technology was developed to achieve an extremely high assembly rate ($>100 \text{ M units h}^{-1}$ [46]) by simultaneously transferring a large number of chips just by one laser pulse. As shown in figure 10(b), an array of laser beams irradiates multiple chips together, which are divided from a single laser beam with the help of a diffractive optical element. Since each beam can transfer one chip, the maximum assembly rate can be multiplied by the number of diffracted beams.

The same as conventional LIFT processes, the high falling speed (e.g. $\sim 540 \text{ m s}^{-1}$ for 10 ns – 1064 nm laser with aluminum as DRL [215, 216]) still becomes a tough problem,

which brings difficulties for controlling the transfer accuracy. A statistical test indicated that the transfer error, which mainly includes the lateral offset and the angular deflection, is positively related to the gap between the stamp and the receiver substrate. Unfortunately, when setting the gap very close, the squeeze-film effect may reduce the kinetic energy of the released chip, which will also affect the transfer accuracy [100]. Therefore, it is difficult to accurately control the placement accuracy of multi-beam lasers. Under practical conditions, affected by many factors such as laser energy fluctuations, inconsistency of multi-beam size/shape, initial alignment deviation, and the heterogeneity of material/geometric properties, etc, some unexpected results might occur after laser irradiation, including the failure of chip peeling, unacceptable deviation, and chip damage (creaking), etc. The industry usually uses the experimental trial-and-error method to get a better combination of process parameters. However, up to now, MPLET can achieve a success rate of only about 90% [46], which is far below the desired value. Due to the lack of in-depth research on transfer mechanisms, it is still unable to fundamentally reveal the reasons for the transfer failure, as well as the influence of process parameters on transfer results. Therefore, it still requires a lot of effort in experimental and

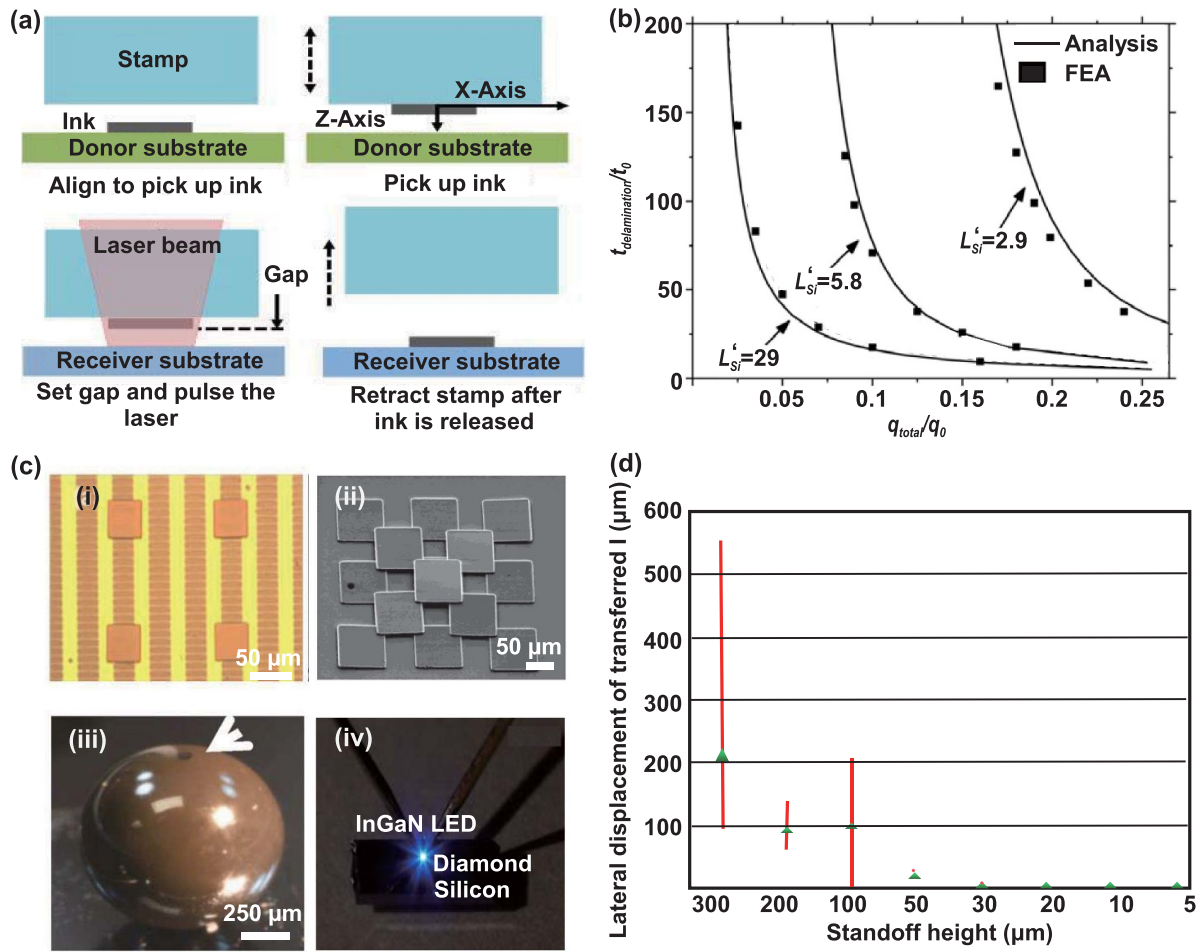


Figure 11. (a) Schematic illustration of a type of laser-induced forward transfer technique based on thermal mismatch. Reprinted from [99], Copyright (2012), with permission from Elsevier. (b) The scaling law for the laser pulse time for delamination of the stamp–chip interface. Reprinted by permission from Springer Nature Customer Service Centre GmbH: Springer Nature, Flex. Electron. [183], © 2018. (c) Examples of micro-structures constructed by a LIFT-TM technique based on thermal mismatch [99]. (i) Photomicrograph of silicon squares printed on a silicon substrate with gold traces; (ii) Three-dimensional pyramid structures consisting of silicon chips; (iii) An example of printing micro-structures on a ceramic sphere; (iv) Functional microLEDs printed on a CVD-grown polycrystalline diamond on a silicon substrate. (d) Maximum lateral displacements error of transferred chips as a function of the standoff height. Reprinted from [99], Copyright (2012), with permission from Elsevier.

theoretical research to gradually improve the process stability and reliability.

Another limitation of BB-LIFT is that the stamp cannot be reused due to the irreversible ablation of DRL. As shown in figure 11(c), for the cost-benefit consideration, a reusable BB-LIFT technique was developed [46] based on an ingenious design of a reusable stamp, which is composed of a microcavity with a metal layer attached to the cavity wall and an elastic adhesive stamp with microstructures for encapsulating the microcavity and bonding the chip. Under the irradiation of an 808 nm laser (~ 400 mW), the metal layer absorbs the laser to generate heat, which causes the expansion of the internal air of the cavity due to the rapid temperature rise (~ 100 °C in 100 ms). The deformed stamp could largely reduce its adhesion (adhesion switching ratio >1000). Figure 10(d) shows the ability to print a microLED chip ($400 \times 200 \times 90$ μm) on a variety of tack-free flat or curved surfaces, such as a PDMS column array with a column diameter of 100 μm and a column pitch of 150 μm (figure 10(d-I)), a steel ball with a diameter of

1 mm (figure 10(d-II)), and a sheet of paper (figure 10(d-III)). Figure 10(d-iv) shows microLED chips were transferred onto the curvilinear surface of a Scindapsus leaf to form a letter ‘Z’. The same square microLED chips were printed on a mobile-phone shell with a pit to form a letter ‘P’, as shown in figure 10(d-V). These presentations demonstrated the powerful ability to accurately place microLED chips regardless of the receiver surface properties. Nevertheless, how to further reduce the geometric sizes of this cleverly designed stamp with high manufacturing accuracy is a big problem for this technique.

4.2.3. Laser-induced forward transfer based on the thermal mismatch. A new LIFT-type technique based on the thermal mismatch of a multi-layer structure (LIFT-TM) combines the accuracy and versatility of traditional transfer printing processes in picking up chips directly and selectively from their growth/fabrication substrates and has the advantage of

conventional LIFT processes to realize noncontact placing process [98, 218–220]. As shown in figure 11, the LIFT-TM utilizes an elastomeric stamp made of PDMS to selectively pick up chips to be transferred. Then, a NIR pulsed laser is focused on the stamp-chip interface and the chip absorbs the laser and generates heat, which makes the chip released from the stamp resulting from different thermomechanical responses of the chip and the PMDS stamp [98]. An accurate thermomechanical model has been developed to establish a scaling law governing the delamination of a chip, as shown in figure 11(b). The energy release rate at the stamp/chip interface is characterized by $\frac{t_{\text{delamination}}}{t_0} = f\left(\frac{q_{\text{total}}}{q_0}, L'_{\text{si}}\right)$, which is a function of total heat flux q_{total}/q_0 and the normalized width of the silicon chip ($L'_{\text{si}} = c_{\text{PDMS}}\rho_{\text{PDMS}}L_{\text{chip}}/(c_{\text{chip}}\rho_{\text{chip}}h_{\text{chip}})$), where $t_{\text{delamination}}$ and q_{total} are the delamination time and total heat flux, L_{chip} is the width of the chip, c_i ($i = \text{PDMS, chip}$) is the specific heat of stamp and chip, ρ_i ($i = \text{PDMS, chip}$) is the mass density of stamp and chip, t_0 , q_0 are the normalized characteristic time, normalized heat flux, and normalized width determined by properties of the stamp, chip and their interfaces in the system, respectively. Thus, theoretical models can serve as powerful tools for determining the critical process parameters, estimating the temperature, and calculating stresses at the interface.

Extensive viability tests were conducted by using a laser with an 805-nm wavelength, which demonstrated the wide compatibility of various surface characteristics of the receiver and the ability to place ultrathin microstructures [99]. Figure 11(c-i) shows examples of an array of silicon chips that were transferred onto a silicon substrate to bridge gold traces. Multiple silicon chips ($100\ \mu\text{m} \times 100\ \mu\text{m} \times 3\ \mu\text{m}$) were successfully printed layer by layer with high precision for the construction of 3D assemblies in figure 11(c-ii). To demonstrate the ability to transfer chips to non-flat substrates, a 320-nm-thick silicon chip was printed on a ceramic microsphere (figure 11(c-iii)). Moreover, the microLED chip is still functional after being placed on a silicon substrate (figure 11(c-iv)). Notwithstanding all this, a foreseeable challenge of this process is the limitation to chip materials. Chip materials with high reflectivity or low absorptive to the NIR laser are incompatible. Also, the required high temperature ($100\ ^\circ\text{C}$ – $200\ ^\circ\text{C}$) at the interface may bring damage to the chips. Also, the shear forces caused by the thermal mismatch cause a relatively long delamination time ($\sim 0.5\ \text{ms}$), which may limit the maximum transfer efficiency. Moreover, much research still needs to be done to quantitatively discuss important process parameters and their impact on the process accuracy. Figure 11(d) shows the maximum lateral error after transfer versus the receiving substrate spacing (i.e. standoff height [99]). The transfer error can be negligible when the standoff height is less than $20\ \mu\text{m}$. However, other factors have not been carried out yet.

4.3. Self-assembly techniques

Self-assembly is a process that a massive number of independent components can spontaneously form into ordered

arrangements. The traditional mass assembly techniques generally include four steps, i.e. positioning the donor substrate, picking up, positioning the receiver substrate, and placing. Each of these steps has become extraordinarily difficult when facing the massive number of chips with microscale sizes. A significant difference from the working principle of the aforementioned techniques is that the self-assembly technique requires only one step, i.e. placing the microLED chips in the corresponding fluid medium, which enables the microLED chips to be oriented and positioned in a predetermined location through medium transport and shape recognition. As an ingenious approach, self-assembly techniques use several physical force fields that can orient individual chips and filter out all parts that are in the wrong positions. These abilities may well greatly simplify the whole working procedures to largely increase the transfer efficiency. According to the specific physical fields for transferring and orientation, self-assembly techniques can be divided into two categories, i.e. fluid self-assembly, and magnetic/electric self-assembly.

4.3.1. Fluid self-assembly. Representative fluid self-assembly is illustrated in figure 12(a). A specially designed receiver substrate is placed in a self-assembly bath at a specific angle such as $\sim 30^\circ$ to help the chips move gently due to gravity [221]. Once freestanding microLED chips are submerged in the liquid medium (e.g. acidic ethylene glycol), the liquid medium allows microLED chips to move freely until they come into touch with the molten alloy at the predetermined locations to form a stable bonding. microLEDs are positioned and oriented by shape recognition and surface tension-driven self-alignment. Shape recognition is achieved through complementary shapes (pits) of microLEDs on the receiver substrate [222, 223]. Thus, as shown in figure 12(b), only microLEDs with specific shapes, such as a round shape with a $160\ \mu\text{m}$ radius, can be adaptable for shape recognition. In contrast, surface tension-driven self-alignment uses capillary forces of the molten alloy on the substrate (figure 12(c) [224]). At first, a confined liquid drop (molten alloy) is arranged in a pre-designed pattern (figure 12(c-i)). The molten alloy spontaneously forms a meniscus shape due to capillary forces (figures 12(c-ii, iii)). This action tends to align the chip to the target location (figure 12(c-iv)). Generally, an essential design criterion for capillary self-alignment is that the liquid molten alloy constrained by a receptor and a chip (or a part of it) possesses sufficient high potential energy to recover to its equilibrium shape so that this recovery process can sustain the self-aligning motion. Their strong abilities of the orientation of microLEDs have been well demonstrated. The results indicate fluid self-assembly can achieve a 97% transfer rate with self-assembly rate of $40\ 000\ \text{units h}^{-1}$ for $100\ \mu\text{m}$ -sized components if only mechanical positioning (without electrical connections) is considered [107].

To further promote transfer efficiency, Jacobs *et al* introduced an automated RTR fluid self-assembly system, as illustrated in figure 12(d). This system contains two parts [25, 80, 102]: (a) RTR assembly part (shaded in gray), which

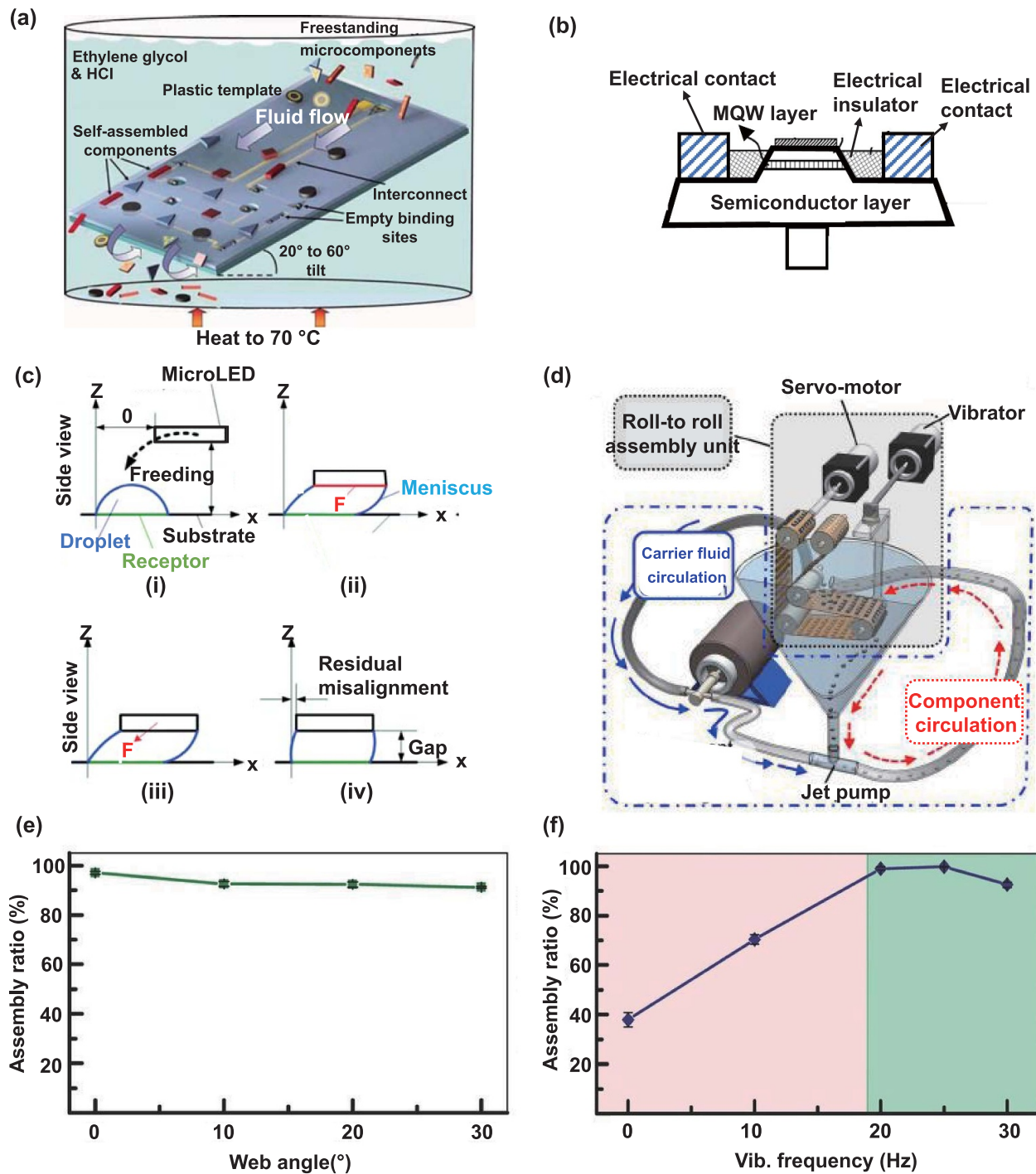


Figure 12. (a) Illustration of fluid self-assembly process. (b) An example of the specially designed microLED in fluid self-assembly process [103]. (a), (b) Reproduced with permission from [103]. (c) Schematic illustrating the principles of surface-tension-driven self-alignment. (d) Illustration of RTR fluid self-assembly process. (e)–(f) Web angle and vibration frequency as a function of assembly rate in the RTR fluid self-assembly process. (d)–(f) [25] John Wiley and Sons.

consists of motor, rollers, customized agitator, and polyimide web with precisely controlled process parameters such as web moving speed and tension. (b) The component recovery and dispensing unit (shaded in blue), primarily utilizes the principle of a jet pump to transport un-assembled chips upward in

a closed fluid channel, releasing them above the substrate and tumbling them down under gravity. It has also been revealed that the RTR fluid self-assembly process requires strict control of gravity (i.e. the tilt angle of the receiving substrate) and vibration frequency (0–30 Hz). The effect of the web angle on

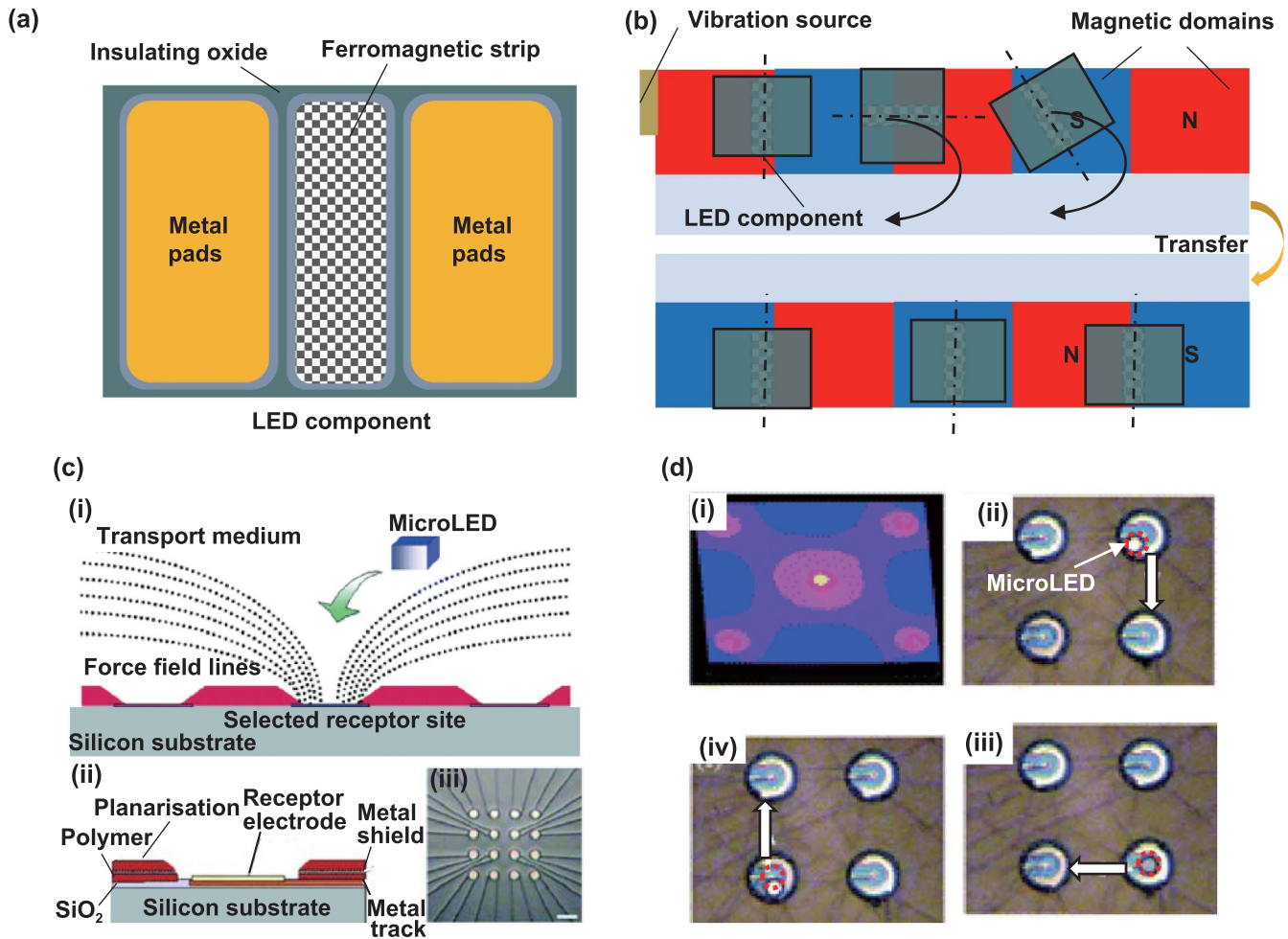


Figure 13. (a) An example of a microLED with ferromagnetic material. (b) A programmed magnetic self-assembly process. (c) Schematic representation of the field configured assembly process: (i) The selected receptor electrode is electrically biased and initiates an electric field at the Si substrate, which allows the transport and assembly of a chip; (ii) Lateral view of the layer structure of a field configured assembly; (iii) A photomicrograph of the receptor array. The interconnecting tracks of the receptor electrodes are visible underneath the overlying metal shield and the polymer planarization layer. (d) An example of a microLED chip being successfully integrated by configured electric fields. (c), (d) Reprinted with permission from [229]. Copyright (2004) American Chemical Society.

the assemble rate is shown in figure 12(e). A slight decrease in assembly rate can be observed at higher tilt angles, mainly because the chips start sliding too fast, and some of them slide over the solder bumps, instead of being captured immediately. The assembly rate as a function of vibrational frequency is shown in figure 12(d), the optimal frequency should be >20 Hz. Otherwise, at a too low vibration frequency, the agitation is not strong enough to overcome non-specific adhesion and gravity, and most chips remain stationary. Through a series of optimizations, RTR fluid self-assembly can achieve a assemble efficiency of 15 000 chips (square $500\ \mu\text{m}$ chips) per hour with a yield rate of $>99\%$.

Looking ahead, a lot of further work still needs to be done on fluid self-assembly techniques to meet the requirements of mass transfer techniques. On the one hand, most of the existing fluidic self-assembly techniques stay on some simple shapes of microLED chips (e.g. above-mentioned round and square). Therefore, to improve the universality, more complex 3D geometries of microLED chips need to be investigated [225]. On

the other hand, further optimization of chip size, solder materials and assembly automation systems is necessary. Typically, to address interconnect stability and improve transfer yields, solder stacks with low melting point shells (e.g. $\text{Bi}_{33.7}\text{In}_{66.3}$ solder shell [222, 226]) can be further introduced so that after assembly at low temperatures, a short reflow step at a higher temperature can be used to form the alloy to increase the melting point of the interconnect.

4.3.2. Magnetic/electric fluid self-assembly. A stronger self-alignment ability is the most salient feature of the magnetic/electric assembly techniques. For the magnetic self-assembly, a magnetic field between the microLEDs and the receptor site is required. As shown in figures 13(a), a thin strip of ferromagnetic material (e.g. nickel, iron, etc) is deposited at the microLED surface as a p-type contact and the adjacent metal pad acts as an n-type contact [227]. For permanently magnetized hard magnetic materials, self-assembly

may not require an external magnetic field. By contrast, the magnetization of soft magnetic materials is highly dependent on the external magnetic field and they tend to revert to a non-magnetized state with the removal of the magnetic field. Thus, magnetic self-assembly of soft or superparamagnetic components requires an external magnetic field. During the magnetic assembly process, the microLED chips are placed on a vibrating magnetic substrate (figure 13(b)). Magnets with opposite polarity are arranged adjacent to each other on the table. The center of the edge between the adjacent magnets becomes the node of maximum magnetic field strength. Once the magnetic microLED chips are placed on the vibrating magnetic table, they can be randomly dispersed by vibration. With the assistance of the magnetic field, the chips are arranged parallel to each other at the nodes of maximum magnetic field strength to achieve the self-assembly process.

In electric self-assembly, a phenomenon of electrophoretic transport (charged particles move toward the electrode opposite to their electric polarity) is applied, which makes the chips move and locate at the selected receptor sites. As shown in figure 13(c-i), O'Riordan *et al* recently reported a preliminary idea of the programmable electric self-assembly (i.e. field configured assembly, FCA [228, 229]), where the electric fields can be configured by selective addressing receptor sites pre-patterned onto a silicon substrate. The silicon substrate consists of 4×4 circular arrays of receptor electrodes (100 μm diameter and 250 μm spacing) with counter electrodes (500 μm diameter) located at the four corners of each array (figure 13(c-ii)). The conductive interconnect tracks connect each electrode to a unique contact pad located at the periphery of the chip (figures 13(c-ii, iii)). The electric field simulation in figure 13(d-I) shows that an electric field can indeed be generated between a unique receptor electrode point on the silicon chip and the counter electrodes at the four corners with a magnitude sufficient to affect electric-field-assisted device transmission. Figures 13(D-ii)–(D-iv) shows a successful transmission of a microLED chip with a 50 μm diameter. Initially, a microLED chip was located at the top right receptor electrode, and after applying an electrical bias of approximately 20 V to each adjacent target receptor electrode, in turn, the chip was delivered to the bottom right receptor finally. It is worth noting that it is still necessary to ensure the shape of the microLEDs is commensurate with the receptor.

Due to the extremely high requirement on the success rate for mass transfer, until now, the above self-assembly technologies cannot be applied in large-scale production, therefore, transfer yields related data are still available. There are still many technical problems to be solved to avoid the missed chip as little as possible. Thus, deep studies of the effect of process parameters on alignment accuracy are needed, such as the strength of the magnetic/electrostatic field, the distance and direction between the chip and site, the size and shape of the chips, and the degree of magnetization/electrostatics. Another limitation is the microLED chips for self-assembly need special structural characteristics and functional properties. For example, magnetic self-assembly can only be applied with microLED chips with magnetic components, while electric fluid self-assembly requires charged microLED chips.

Also how to transfer different colors of RGB microLED chips separately is currently unclear.

5. Conclusion and future perspective

Mass transfer technique offers the possibility of large-scale, highly efficient and high-yield heterogeneous integration of microLED arrays into spatially organized, functionally arranged 2D and 3D layouts. It creates a number of new applications and industrialization opportunities for next-generation microLED displays and new microLED-based electronics, which are impossible by conventional pick-and-place techniques. In the past decade, the development of mass transfer is generally converging on realizing the following targets: (a) satisfy the needs of cutting-edge applications that hinder from the minuscule size of microLEDs and solve the relevant issues including high accuracy positioning, and selective integration with large numbers; (b) replace the complex, highly expensive, and time-consuming multiple steps of conventional assembly methods with digital/parallel processes to greatly enhance the throughput, cost-efficiency, and manufacturing flexibility; (c) broaden the process window that can enable a deterministic and reliable transfer process and tolerate a little more process variation due to the hardly avoidable fabrication error for high-reliability requirements.

Recently, various techniques based on ingenious design concepts and processing principles have been established and developed toward the above targets. All these techniques are based on clever manipulation of the interfacial adhesion between the microLED chips and the growth/intermediate substrate. In this review, recent advancements in mass transfer techniques were overviewed. The necessary considerations to properly utilize interfacial adhesion control for desired purposes were summarized. Two essential techniques, which are epitaxial lift-off techniques and pick-and-place techniques were introduced from basic mechanism to the state-of-the-art demonstrations. Despite recent progress, there is a continuing need for further development before these mass transfer techniques become reliable manufacturing candidates for the industrialized manufacturing of microLED displays.

Firstly, a further in-depth study of interfacial adhesion mechanisms is necessary. The essential relationship between the process parameters and interface reaction (e.g. adhesion strength, fracture mechanics, and chip peeling/floating state) can undoubtedly provide quantitative guidance for the high reliability of mass transfer. For example, as in the case of epitaxial lift-off techniques, a complicated film delamination mechanism involves the synergistic effects of applied physical fields (e.g. mechanical loads and laser irradiations) and chemical reactions (e.g. ablation in LLO, chemical etching in CLO), thus building complex coupling models of physics, mechanics, and chemistry is essential. As another example, in fluid self-assembly, the interface surface energy is an important parameter needed to be carefully considered, however, there still lacks a direct measurement method at a microscopic scale, which may increase the uncertainty of this technique

resulting from some indeterminate process parameters (can only be determined by trial and error). The continuing efforts to develop more simple and accurate methods for interface bonding energy measurement and establish corresponding theoretical models are still necessary, which will facilitate a more deep understanding of some interface microscopic phenomena.

Secondly, although lots of small-area transfer schemes have been extensively verified, a further improvement in the reliability, accuracy, and efficiency of large-area transfer techniques is still an area of tremendous opportunities. For contact μ TP techniques, the parallel transfer can only be realized by expanding the number of transfer heads. However, the micro-column of an elastic stamp tends to collapse during contact transfer, and it is difficult to make individual transfer heads in a small size for an electromagnetic or electrostatic stamp. These challenges can probably be overcome by further optimization of the structural design and manufacturing processes of transfer heads. For laser non-contact transfer techniques, although the time for a single transfer is considerably short, the transfer rate is still greatly limited by the moving speed of the laser spot and the number of chips that can be transferred by a single spot. Increasing the moving speed of the spot by vibrating mirror scanning (the high-speed vibrating mirror can achieve tens of thousands of scans per second) and the number of spot arrays by optical projection mask and optical space modulation is the future trend. As for the magnetic/electric fluid self-assembly, arrayed magnetic and electric fields need to be introduced. And for contact μ TP techniques, the parallel transfer can only be realized by expanding the number of transfer heads. However, the micro-column of an elastic stamp tends to collapse during contact transfer, and it is difficult to make individual transfer heads in a small size for an electromagnetic or electrostatic stamp.

For achieving high reliability, the development of high precision micro-fabrication/position technologies and material preparations for chips, transfer stamps, and receiver substrates/solders are hotspots, since lots of mass transfer techniques rely on some specific properties/shapes at specified positions. For example, the fluid self-assembly technique has special requirements for adhesives, which ask for better fluidity, high bonding selectivity between assembled and unassembled surfaces, and acid/high-temperature resistance considering subsequent processes. However, the present acrylate heat-curing adhesives and solders do not fully meet these requirements. In addition, to improve the transfer accuracy, the introduction of optical position calibration systems or auxiliary positioning technologies may become a focal point. Until now, the optical alignment for contact μ TP is still challenging, and further improving sensor resolution and marking stamp materials with better contrast is necessary to achieve a brighter fiducial mark. On the other hand, Emine Eda Kuran *et al* have proved that LIFT can combine with a magnetic-assisted alignment technology. The chip was transferred by LIFT firstly, while the autonomous positioning can be achieved with the help of magnetic traction.

Further exploration of cost-efficient mass transfer techniques is full of challenges as well as opportunities. The development of reversible laser-assisted μ TP has important practical significance which can easily achieve high throughput for large-scale and high-output manufacturing with the help of parallel laser systems and automated platforms. To reduce fabrication costs, a reusable stamp is essential. However, the laser-induced physical/chemical modifications of the reusable stamp need to be carefully controlled to avoid undesirable distortion or damage. In addition, most of these stamps rely on phase transition of smart materials (e.g. SMP), therefore how to further reduce response time through technical innovation of materials and configurations is worth investigating. Also, inventions that can simplify processing steps to reduce the manufacturing cost are favorable. For example, the development of selective epitaxial lift-off processes (specific microLEDs are directly transferred from the source substrate to the target substrate) may probably avoid a series of intermediate steps. Moreover, decreasing the cost of mass transfer equipment deserves the same consideration. The commonly used excimer laser systems (cost millions of dollars) may be replaced by relatively low-cost laser systems (solid-state laser or fiber lasers).

Finally, looking into the future, with a series of tremendous efforts, mass transfer techniques can prepare microLEDs displays of various sizes at low cost. As a result, OLED and LED displays will be replaced, as microLEDs have more advantages for OLEDs and LCDs. The application of microLEDs is not limited to displays, but also will be combined with optical communication, wearable, smart lights and other applications. Especially, high-end glass-based AR/VR can provide a high brightness of 100 000 nits, high ppi > 2000, and high contrast of 100 000:1 to view in an outdoor environment. This brightness cannot be provided by OLED. Since wearable micro-LEDs can be prepared in large areas, wearable microLEDs can be widely used not only for biomedical applications (including biosensors, medical devices and optogenetic stimulators) but also for large area detection in devices such as aircraft and vehicles. Also, higher brightness than broad-area OLED at high current density is a significant advantage of microLEDs in the application of VLC, as one of the disadvantages of VLC is the short communication distance. Therefore, in the future, integrated microLEDs can achieve higher data transmission (e.g. 12Gb/s [230, 231]), leading to an accelerated convergence of communication techniques interactions.

In summary, the excellent performance of will certainly revolutionize the applications of displays soon. A lot of potentially disruptive technologies for mass production of microLED displays may be developed by a further in-depth study of laser-induced interface phenomena, multi-scale adhesion-controlled interface, micro/nanomanufacturing technology, etc. These considerations suggest that this field of study will remain active and dynamic, promising more versatile, effective, and cost-efficient mass transfer techniques for microLED displays fabrication in the near future.

Acknowledgments

This study was supported by the National Natural Science Foundation of China (51925503, 52188102, 52105576), and Natural Science Foundation of Hubei Province of China (2020CFA028). The general characterization facilities are provided by the Flexible Electronics Manufacturing Laboratory in Comprehensive Experiment Center for Advanced Manufacturing Equipment and Technology at Huazhong University of Science and Technology. The authors declare that they have no conflict of interest.

ORCID iD

YongAn Huang  <https://orcid.org/0000-0001-7713-8380>

References

- [1] Meng W Q *et al* 2021 Three-dimensional monolithic micro-LED display driven by atomically thin transistor matrix *Nat. Nanotechnol.* **16** 1231–6
- [2] Jin S X, Li J, Li J Z, Lin J Y and Jiang H X 2000 GaN microdisk light emitting diodes *Appl. Phys. Lett.* **76** 631–3
- [3] Z L L *et al* 2018 Heterogeneous integration of microscale GaN light-emitting diodes and their electrical, optical, and thermal characteristics on flexible substrates *Adv. Mater. Technol.* **3** 1700239
- [4] Kim T I *et al* 2012 High-efficiency, microscale GaN light-emitting diodes and their thermal properties on unusual substrates *Small* **8** 1643–9
- [5] Parbrook P J, Corbett B, Han J, Seong T Y and Amano H 2021 Micro-light emitting diode: from chips to applications *Laser Photonics Rev.* **15** 2000133
- [6] Chen Z, Yan S K and Danesh C 2021 MicroLED technologies and applications: characteristics, fabrication, progress, and challenges *J. Appl. Phys.* **54** 123001
- [7] Lee H E, Shin J H, Park J H, Hong S K, Park S H, Lee S H, Lee J H, Kang I S and Lee K J 2019 Micro light-emitting diodes for display and flexible biomedical applications *Adv. Funct. Mater.* **29** 1808075
- [8] Zhang L, Ou F, Chong W C, Chen Y J, Zhu Y K and Li Q M 2018 31.1: *Invited Paper*: monochromatic active matrix micro-LED micro-displays with >5000 dpi pixel density fabricated using monolithic hybrid integration process *SID Symp. Digest of Technical Papers* vol 49 pp 333–6
- [9] Kim J *et al* 2017 Miniaturized battery-free wireless systems for wearable pulse oximetry *Adv. Funct. Mater.* **27** 1604373
- [10] Lochner C M, Khan Y, Pierre A and Arias A C 2014 All-organic optoelectronic sensor for pulse oximetry *Nat. Commun.* **5** 5745
- [11] Jang T M *et al* 2020 Expandable and implantable bioelectronic complex for analyzing and regulating real-time activity of the urinary bladder *Sci. Adv.* **6** eabc9675
- [12] Lee H E *et al* 2019 Wireless powered wearable micro light-emitting diodes *Nano Energy* **55** 454–62
- [13] Wang L *et al* 2021 1.3 GHz E-O bandwidth GaN-based micro-LED for multi-gigabit visible light communication *Photon. Res.* **9** 792–802
- [14] Koester R, Sager D, Quitsch W A, Pfingsten O, Poloczek A, Blumenthal S, Keller G, Prost W, Bacher G and Tegude F J 2015 High-speed GaN/GaN nanowire array light-emitting diode on silicon(111) *Nano Lett.* **15** 2318–23
- [15] Ferreira R X G *et al* 2016 High bandwidth GaN-based micro-LEDs for multi-Gb/s visible light communications *IEEE Photonics Technol. Lett.* **28** 2023–6
- [16] Wasisto H S, Prades J D, Güllink J and Waag A 2019 Beyond solid-state lighting: miniaturization, hybrid integration, and applications of GaN nano- and micro-LEDs *Appl. Phys. Rev.* **6** 041315
- [17] Mei S L, Liu X Y, Zhang W L, Liu R, Zheng L R, Guo R Q and Tian P F 2018 High-bandwidth white-light system combining a micro-LED with perovskite quantum dots for visible light communication *ACS Appl. Mater. Interfaces* **10** 5641–8
- [18] Darlis A R, Cahyadi W A and Chung Y H 2018 Shore-to-undersea visible light communication *Wirel. Pers. Commun.* **99** 681–94
- [19] Lin R Z, Liu X Y, Zhou G F, Qian Z Y, Cui X G and Tian P F 2021 InGaN micro-LED array enabled advanced underwater wireless optical communication and underwater charging *Adv. Opt. Mater.* **9** 2002211
- [20] Li L Z *et al* 2021 Transfer-printed, tandem microscale light-emitting diodes for full-color displays *Proc. Natl Acad. Sci. USA* **118** e2023436118
- [21] Virey E H, Baron N and Bouhamri Z 2019 11–3: Overlooked challenges for microLED displays *SID Symp. Digest of Technical Papers* vol 50 pp 129–32
- [22] Wu Y F, Ma J S, Su P, Zhang L J and Xia B Z 2020 Full-color realization of Micro-LED displays *Nanomaterials* **10** 2482
- [23] Fukushima T, Konno T, Iwata E, Kobayashi R, Kojima T, Murugesan M, Bea J C, Lee K W, Tanaka T and Koyanagi M 2011 Self-assembly of chip-size components with cavity structures: high-precision alignment and direct bonding without thermal compression for hetero integration *Micromachines* **2** 49–68
- [24] Liu Z X, Huang Y A, Liu H M, Chen J K and Yin Z P 2014 Reliable peeling of ultrathin die with multineedle ejector *IEEE Trans. Compon. Packag. Manuf. Technol.* **4** 1545–54
- [25] Park S C, Fang J, Biswas S, Mozafari M, Stauden T and Jacobs H O 2014 A first implementation of an automated reel-to-reel fluidic self-assembly machine *Adv. Mater.* **26** 5942–9
- [26] Virey E H and Baron N 2018 45–1: status and prospects of microLED displays *SID Symp. Digest of Technical Papers* vol 49 pp 593–6
- [27] Liu X Y, Tong C Y, Luo X S, Li W Z and Liu Z J 2019 P-6.8: study of mass transfer for micro-LED manufacturing *SID Symp. Digest of Technical Papers* vol 50 pp 775–8
- [28] Park S C, Fang J, Biswas S, Mozafari M, Stauden T and Jacobs H O 2014 Self-assembly: a first implementation of an automated reel-to-reel fluidic self-assembly machine *Adv. Mater.* **26** 5890
- [29] Zou Q B and Wang Z 2019 Transferring method, manufacturing method, device and electronic apparatus of micro-LED *U.S. Patent* No. 10224308B2
- [30] Xu L Z *et al* 2014 3D multifunctional integumentary membranes for spatiotemporal cardiac measurements and stimulation across the entire epicardium *Nat. Commun.* **5** 3329
- [31] Chun H, Gomez A, Quintana C, Zhang W D, Faulkner G and O'Brien D 2019 A wide-area coverage 35 Gb/s visible light communications link for indoor wireless applications *Sci. Rep.* **9** 4952
- [32] Huang M X, Guan W P, Fan Z B, Chen Z H, Li J Y and Chen B D 2018 Improved target signal source tracking and extraction method based on outdoor visible light communication using a cam-shift algorithm and Kalman filter *Sensors* **18** 4173
- [33] Meitl M A, Zhu Z T, Kumar V, Lee K J, Feng X, Huang Y Y, Adesida I, Nuzzo R G and Rogers J A 2006 Transfer

- printing by kinetic control of adhesion to an elastomeric stamp *Nat. Mater.* **5** 33–38
- [34] Carlson A, Bowen A M, Huang Y G, Nuzzo R G and Rogers J A 2012 Transfer printing techniques for materials assembly and micro/nanodevice fabrication *Adv. Mater.* **24** 5284–318
- [35] Kaltwasser M, Schmidt U, Biswas S, Reiprich J, Schlag L, Isaac N A, Stauden T and Jacobs H O 2018 Core-shell transformation-imprinted solder bumps enabling low-temperature fluidic self-assembly and self-alignment of chips and high melting point interconnects *ACS Appl. Mater. Interfaces* **10** 40608–13
- [36] Biedermann L B, Beechem T E, Ross A J, Ohta T and Howell S W 2010 Electrostatic transfer of patterned epitaxial graphene from SiC(0001) to glass *New J. Phys.* **12** 125016
- [37] Kim S *et al* 2019 Soft nanocomposite electroadhesives for digital micro- and nanotransfer printing *Sci. Adv.* **5** eaax4790
- [38] Um J G, Jeong D Y, Jung Y, Moon J K, Jung Y H, Kim S, Kim S H, Lee J S and Jang J 2019 Active-matrix GaN μ -LED display using oxide thin-film transistor backplane and flip chip LED bonding *Adv. Electron. Mater.* **5** 1800617
- [39] Bian J, Zhou L B Y, Wan X D, Zhu C, Yang B and Huang Y A 2019 Laser transfer, printing, and assembly techniques for flexible electronics *Adv. Electron. Mater.* **5** 1800900
- [40] Kim J Y, Cho Y H, Park H S, Ryou J H and Kwon M K 2019 Mass transfer of microscale light-emitting diodes to unusual substrates by spontaneously formed vertical tethers during chemical lift-off *Appl. Sci.* **9** 4243
- [41] Yoon J *et al* 2010 GaAs photovoltaics and optoelectronics using releasable multilayer epitaxial assemblies *Nature* **465** 329–33
- [42] Cok R S *et al* 2017 Inorganic light-emitting diode displays using micro-transfer printing *J. Soc. Inf. Dis.* **25** 589–609
- [43] Bower C A *et al* 2020 High-brightness displays made with micro-transfer printed flip-chip microLEDs *Proc. IEEE 70th Electronic Components and Technology Conf.* (Orlando, FL: IEEE)
- [44] Gomez D *et al* 2019 Manufacturing capability of micro-transfer printing *Proc. 13th Int. Conf. and Exhibition on Integration Issues of Miniaturized Systems* (Barcelona: IEEE) pp 1–4
- [45] Gomez D, Ghosal K, Moore T, Meitl M A, Bonafede S, Prevatte C, Radauscher E, Trindade A J and Bower C A 2017 Scalability and yield in elastomer stamp micro-transfer-printing *Proc. 67th Electronic Components and Technology Conf.* (Orlando, FL: IEEE)
- [46] Marinov V R 2018 Laser-enabled extremely-high rate technology for μ LED assembly *SID Symp. Digest of Technical Papers* vol 49 pp 692–5
- [47] Wierer J J J and Tansu N 2019 III-nitride micro-LEDs for efficient emissive displays *Laser Photonics Rev.* **13** 1900141
- [48] Zhou X J, Tian P F, Sher C W, Wu J, Liu H Z, Liu R and Kuo H C 2020 Growth, transfer printing and colour conversion techniques towards full-colour micro-LED display *Prog. Quantum Electron.* **71** 100263
- [49] Huang Y G, Hsiang E L, Deng M Y and Wu S T 2020 Mini-LED, Micro-LED and OLED displays: present status and future perspectives *Light Sci. Appl.* **9** 105
- [50] Ho S J, Hsu H C, Yeh C W and Chen H S 2020 Inkjet-printed salt-encapsulated quantum dot film for UV-based RGB color-converted micro-light emitting diode displays *ACS Appl. Mater. Interfaces* **12** 33346–51
- [51] Templier F and Bernard J 2019 18–3: a new approach for fabricating high-performance microLED displays *SID Symp. Digest of Technical Papers* vol 50 pp 240–3
- [52] Lee B J and Khang D Y 2021 Non-deterministic transfer-printing of LED chips with controllable pitch using stretchable elastomeric stamps *Extreme Mech. Lett.* **45** 101287
- [53] Colvin V L, Schlamp M C and Alivisatos A P 1994 Light-emitting diodes made from cadmium selenide nanocrystals and a semiconducting polymer *Nature* **370** 354–7
- [54] Shirasaki Y, Supran G J, Bawendi M G and Bulović V 2013 Emergence of colloidal quantum-dot light-emitting technologies *Nat. Photon.* **7** 13–23
- [55] Han H V *et al* 2015 Resonant-enhanced full-color emission of quantum-dot-based micro LED display technology *Opt. Express* **23** 32504–15
- [56] Pust P, Weiler V, Hecht C, Tücks A, Wochnik A S, Henß A K, Wiechert D, Scheu C, Schmidt P J and Schnick W 2014 Narrow-band red-emitting Sr [LiAl₃N₄]:Eu²⁺ as a next-generation LED-phosphor material *Nat. Mater.* **13** 891–6
- [57] Liu Y T, Lai Y H and Li Y L 2019 23.1: *Invited Paper*: heading to ultimate display with MicroLED *SID Symp. Digest of Technical Papers* vol 50 p 220
- [58] Jung T, Choi J H, Jang S H and Han S J 2019 32–1: *Invited Paper*: review of micro-light-emitting-diode technology for micro-display applications *SID Symp. Digest of Technical Papers* vol 50 pp 442–6
- [59] Horng R H, Chien H Y, Tarntair F G and Wu D S 2018 Fabrication and study on red light micro-LED displays *IEEE J. Electron Devices Soc.* **6** 1064–9
- [60] Li Z, Waldron J, Detchprohm T, Wetzel C, Karlicek R F Jr and Chow T P 2013 Monolithic integration of light-emitting diodes and power metal-oxide-semiconductor channel high-electron-mobility transistors for light-emitting power integrated circuits in GaN on sapphire substrate *Appl. Phys. Lett.* **102** 192107
- [61] Kang C M, Kong D J, Shim J P, Kim S, Choi S B, Lee J Y, Min J H, Seo D J, Choi S Y and Lee D S 2017 Fabrication of a vertically-stacked passive-matrix micro-LED array structure for a dual color display *Opt. Express* **25** 2489–95
- [62] Sun C W, Chao C H, Chen H Y, Chiu Y H, Yeh W Y, Wu M H, Yen H H and Liang C C 2011 71–1: Development of micro-pixelated GaN LED array micro-display system *SID Symp. Digest of Technical Papers* vol 42 pp 1042–5
- [63] Ra Y H, Wang R J, Woo S Y, Djavid M, Sadaf S M, Lee J, Botton G A and Mi Z T 2016 Full-color single nanowire pixels for projection displays *Nano Lett.* **16** 4608–15
- [64] Choi M K, Yang J, Hyeon T and Kim D H 2018 Flexible quantum dot light-emitting diodes for next-generation displays *npj Flex. Electron.* **2** 10
- [65] Supran G J, Song K W, Hwang G W, Correa R E, Scherer J, Dauler E A, Shirasaki Y, Bawendi M G and Bulović V 2015 High-performance shortwave-infrared light-emitting devices using core-shell (PbS–CdS) colloidal quantum dots *Adv. Mater.* **27** 1437–42
- [66] Liu Z J *et al* 2020 Micro-light-emitting diodes with quantum dots in display technology *Light Sci. Appl.* **9** 83
- [67] Cheng C W, Shiu K T, Li N, Han S J, Shi L and Sadana D K 2013 Epitaxial lift-off process for gallium arsenide substrate reuse and flexible electronics *Nat. Commun.* **4** 1577
- [68] Liu Y, Huang Y and Duan X F 2019 Van der Waals integration before and beyond two-dimensional materials *Nature* **567** 323–33

- [69] Yulianto N, Kadja G T M, Bornemann S, Gahlawat S, Majid N, Triyana K, Abdi F F, Wasisto H S and Waag A 2021 Ultrashort pulse laser lift-off processing of InGaN/GaN light-emitting diode chips *ACS Appl. Electron. Mater.* **3** 778–88
- [70] Peng Y Y *et al* 2019 Achieving high-resolution pressure mapping via flexible GaN/ZnO nanowire LEDs array by piezo-phototronic effect *Nano Energy* **58** 633–40
- [71] Sheng X *et al* 2014 Printing-based assembly of quadruple-junction four-terminal microscale solar cells and their use in high-efficiency modules *Nat. Mater.* **13** 593–8
- [72] Xu H H, Yin L, Liu C, Sheng X and Zhao N 2018 Recent advances in biointegrated optoelectronic devices *Adv. Mater.* **30** 1800156
- [73] Ueda T, Ishida M and Yuri M 2011 Separation of thin GaN from sapphire by laser lift-off technique *Jpn. J. Appl. Phys.* **50** 041001
- [74] Zhang Y, Sun Q, Leung B, Simon J, Lee M L and Han J 2011 The fabrication of large-area, free-standing GaN by a novel nanoetching process *Nanotechnology* **22** 045603
- [75] Lin C F, Dai J J, Lin M S, Chen K T, Huang W C, Lin C M, Jiang R H and Huang Y C 2010 An AlN sacrificial buffer layer inserted into the GaN/patterned sapphire substrate for a chemical lift-off process *Appl. Phys. Express* **3** 031001
- [76] Feng X, Cheng H Y, Bowen A M, Carlson A W, Nuzzo R G and Rogers J A 2013 A finite-deformation mechanics theory for kinetically controlled transfer printing *J. Appl. Mech.* **80** 061023
- [77] Zhou H L, Qin W Y, Yu Q M, Cheng H Y, Yu X D and Wu H P 2019 Transfer printing and its applications in flexible electronic devices *Nanomaterials* **9** 283
- [78] Li H C, Wang Z H, Cao Y, Chen Y and Feng X 2021 High-efficiency transfer printing using droplet stamps for robust hybrid integration of flexible devices *ACS Appl. Mater. Interfaces* **13** 1612–9
- [79] Liu X, Cao Y, Zheng K W, Zhang Y C, Wang Z H, Chen Y H, Chen Y, Ma Y J and Feng X 2021 Liquid droplet stamp transfer printing *Adv. Funct. Mater.* **31** 2105407
- [80] Biswas S, Mozafari M, Stauden T and Jacobs H O 2016 Surface tension directed fluidic self-assembly of semiconductor chips across length scales and material boundaries *Micromachines* **7** 54
- [81] Bartlett M D, Croll A B, King D R, Paret B M, Irschick D J and Crosby A J 2012 Looking beyond fibrillar features to scale gecko-like adhesion *Adv. Mater.* **24** 1078–83
- [82] Cheng H, Li M, Wu J, Carlson A, Kim S, Huang Y, Kang Z, Hwang K C and Rogers J A 2013 A viscoelastic model for the rate effect in transfer printing *J. Appl. Mech.* **80** 041019
- [83] Zhang H and Rogers J A 2019 Recent advances in flexible inorganic light emitting diodes: from materials design to integrated optoelectronic platforms *Adv. Opt. Mater.* **7** 1800936
- [84] Konagai M, Sugimoto M and Takahashi K 1978 High efficiency GaAs thin film solar cells by peeled film technology *J. Cryst. Growth* **45** 277–80
- [85] Wong W S, Sands T, Cheung N W, Kneissl M, Bour D P, Mei P, Romano L T and Johnson N M 1999 Fabrication of thin-film InGaN light-emitting diode membranes by laser lift-off *Appl. Phys. Lett.* **75** 1360–2
- [86] Koma A 1992 Van der Waals epitaxy—a new epitaxial growth method for a highly lattice-mismatched system *Thin Solid Films* **216** 72–76
- [87] Jeong J *et al* 2021 Transferable, flexible white light-emitting diodes of GaN p - n junction microcrystals fabricated by remote epitaxy *Nano Energy* **86** 106075
- [88] Dean C R *et al* 2010 Boron nitride substrates for high-quality graphene electronics *Nat. Nanotechnol.* **5** 722–6
- [89] Fan S D, Vu Q A, Tran M D, Adhikari S and Lee Y H 2020 Transfer assembly for two-dimensional van der Waals heterostructures *2D Mater.* **7** 022005
- [90] Cheung Y F, Li K H and Choi H W 2016 Flexible free-standing III-nitride thin films for emitters and displays *ACS Appl. Mater. Interfaces* **8** 21440–5
- [91] Delmdahl R and Fechner B 2010 Large-area microprocessing with excimer lasers *Appl. Phys. A* **101** 283–6
- [92] Delmdahl R, Pätzl R, Brune J, Senczuk R, Gößler C, Moser R, Kunzer M and Schwarz U T 2012 Line beam processing for laser lift-off of GaN from sapphire *Phys. Status Solidi a* **209** 2653–8
- [93] Kim J, Kim J H, Cho S H and Whang K H 2016 Selective lift-off of GaN light-emitting diode from a sapphire substrate using 266-nm diode-pumped solid-state laser irradiation *Appl. Phys. A* **122** 305
- [94] Krause S, Miclea P T and Seifert G 2015 Selective femtosecond laser lift-off process for scribing in thin-film photovoltaics *J. Laser Micro Nanoeng.* **10** 274–8
- [95] Kim S *et al* 2010 Microstructured elastomeric surfaces with reversible adhesion and examples of their use in deterministic assembly by transfer printing *Proc. Natl Acad. Sci. USA* **107** 17095–100
- [96] Bibl A, Higginson J A, Law H F S and Hu H H 2013 Micro device transfer head heater assembly and method of transferring a micro device *U.S. Patent No. 8,349,116*
- [97] Sakariya K V, Bibl A and Hu H H 2015 Active matrix display panel with ground tie lines *U.S. Patent No. 20150179703*
- [98] Li R, Li Y H, Lü C F, Song J Z, Saeidpouraza R, Fang B, Zhong Y, Ferreira P M, Rogers J A and Huang Y G 2012 Thermo-mechanical modeling of laser-driven non-contact transfer printing: two-dimensional analysis *Soft Matter* **8** 7122–7
- [99] Saeidpourazar R, Sangid M D, Rogers J A and Ferreira P M 2012 A prototype printer for laser driven micro-transfer printing *J. Manuf. Process.* **14** 416–24
- [100] Miller R, Marinov V, Swenson O, Chen Z G and Semler M 2012 Noncontact selective laser-assisted placement of thinned semiconductor dice *IEEE Trans. Compon. Packag. Manuf. Technol.* **2** 971–8
- [101] Chang T C, Tsao Y C, Chen P H, Tai M C, Huang S P, Su W C and Chen G F 2020 Flexible low-temperature polycrystalline silicon thin-film transistors *Mater. Today Adv.* **5** 100040
- [102] Park S C, Fang J, Biswas S, Mozafari M, Stauden T and Jacobs H O 2015 Approaching roll-to-roll fluidic self-assembly: relevant parameters, machine design, and applications *J. Microelectromech. Syst.* **24** 1928–37
- [103] Saeedi E, Kim S and Parviz B A 2008 Self-assembled crystalline semiconductor optoelectronics on glass and plastic *J. Micromech. Microeng.* **18** 075019
- [104] Sasaki K, Schuele P J, Ulmer K and Lee J J 2017 System and method for the fluidic assembly of emissive displays *U.S. Patent No. 20170133558*
- [105] Cho S, Lee D and Kwon S 2019 Fluidic self-assembly transfer technology for micro-LED display *Proc. 20th Int. Conf. on Solid-State Sensors, Actuators and Microsystems & Eurosensors XXXIII* (Berlin: IEEE) pp 402–4
- [106] Feng X, Meitl M A, Bowen A M, Huang Y G, Nuzzo R G and Rogers J A 2007 Competing fracture in kinetically controlled transfer printing *Langmuir* **23** 12555–60
- [107] Stauth S A and Parviz B A 2006 Self-assembled single-crystal silicon circuits on plastic *Proc. Natl Acad. Sci. USA* **103** 13922–7
- [108] Marinov V R, Swenson O, Atanasov Y and Schneck N 2013 Laser-assisted ultrathin die packaging: insights from a process study *Microelectron. Eng.* **101** 23–30

- [109] Choi M, Jang B, Lee W, Lee S, Kim T W, Lee H J, Kim J H and Ahn J H 2017 Stretchable active matrix inorganic light-emitting diode display enabled by overlay-aligned roll-transfer printing *Adv. Funct. Mater.* **27** 1606005
- [110] Wang C J *et al* 2020 Programmable and scalable transfer printing with high reliability and efficiency for flexible inorganic electronics *Sci. Adv.* **6** eabb2393
- [111] Jiang H X, Jin S X, Li J, Shakya J and Lin J Y 2001 III-nitride blue microdisplays *Appl. Phys. Lett.* **78** 1303–5
- [112] Park S I *et al* 2009 Printed assemblies of inorganic light-emitting diodes for deformable and semitransparent displays *Science* **325** 977–81
- [113] Lin J Y and Jiang H X 2020 Development of microLED *Appl. Phys. Lett.* **116** 100502
- [114] Ozden I, Diagne M, Nurmikko A V, Han J and Takeuchi T 2001 A matrix addressable 1024 element blue light emitting InGaN QW diode array *Phys. Status Solidi a* **188** 139–42
- [115] Chong W C, Cho W K, Liu Z J, Wang C H and Lau K M 2014 1700 pixels per inch (PPI) passive-matrix micro-LED display powered by ASIC *Proc. 2014 IEEE Compound Semiconductor Integrated Circuit Symp.* (La Jolla, CA: IEEE) pp 1–4
- [116] Fan J, Lee C Y, Chen S J, Gang L M, Jun Z L, Yang S, Cai L M, Fei X H and Nian L 2019 30.2: *Invited Paper*: a RGB chip full color active matrix micro-LEDs transparent display with IGZO TFT backplane *SID Symp. Digest of Technical Papers* **50** 326–8
- [117] Delmdahl R, Pätzelt R and Brune J 2013 Large-area laser-lift-off processing in microelectronics *Phys. Proc.* **41** 241–8
- [118] Huang Y A *et al* 2021 Programmable robotized ‘transfer-and-jet’ printing for large, 3D curved electronics on complex surfaces *Int. J. Extremes Manuf.* **3** 045101
- [119] Kelly M K, Ambacher O, Dimitrov R, Handschuh R and Stutzmann M 1997 Optical process for liftoff of group III-nitride films *Phys. Status Solidi a* **159** R3–R4
- [120] Xu J, Zhang R, Gu S L, Xiu X Q, Shen B, Shi Y, Liu Z G and Zheng Y D 2001 Study of the laser lift-off technology of GaN films from sapphire substrates *Proc. 6th Int. Conf. on Solid-State and Integrated Circuit Technology* (Shanghai, China: IEEE) pp 1179–82
- [121] Wang X T *et al* 2012 193 nm excimer laser lift-off for AlGaIn/GaN high electron mobility transistors *J. Vac. Sci. Technol. B* **30** 051209
- [122] Kelly M K, Ambacher O, Dahlheimer B, Groos G, Dimitrov R, Angerer H and Stutzmann M 1996 Optical patterning of GaN films *Appl. Phys. Lett.* **69** 1749–51
- [123] Hayes G J and Clemens B M 2015 Laser liftoff of gallium arsenide thin films *MRS Commun.* **5** 1–5
- [124] Tavernier P R and Clarke D R 2001 Mechanics of laser-assisted debonding of films *J. Appl. Phys.* **89** 1527–36
- [125] Wang M Q, Wang Y, Sun Y J, Zhang G Y, Tong Y Z and Duan H L 2012 Thermo-mechanical solution of film/substrate systems under local thermal load and application to laser lift-off of GaN/sapphire structures *Int. J. Solids Struct.* **49** 1701–11
- [126] Rethfeld B, Ivanov D S, Garcia M E and Anisimov S I 2017 Modelling ultrafast laser ablation *J. Phys. D: Appl. Phys.* **50** 193001
- [127] Yulianto N *et al* 2021 Wafer-scale transfer route for top-down III-nitride nanowire LED arrays based on the femtosecond laser lift-off technique *Microsyst. Nanoeng.* **7** 32
- [128] Bornemann S, Yulianto N, Spende H, Herhani Y, Prades J D, Wasisto H S and Waag A 2020 Femtosecond laser lift-off with sub-bandgap excitation for production of free-standing GaN light-emitting diode chips *Adv. Eng. Mater.* **22** 1901192
- [129] Ueda T, Ishida M and Yuri M 2003 Laser lift-off of very thin AlGaIn film from sapphire using selective decomposition of GaN interlayer *Appl. Surf. Sci.* **216** 512–8
- [130] Bornemann S, Yulianto N, Meyer T, Güllink J, Margenfeld C, Seibt M, Wasisto H S and Waag A 2018 Structural modifications in free-standing InGaIn/GaN LEDs after femtosecond laser lift-off *Multidiscip. Digit. Publ. Inst. Proc.* **2** 897
- [131] Lee K, Zimmerman J D, Xiao X, Sun K and Forrest S R 2012 Reuse of GaAs substrates for epitaxial lift-off by employing protection layers *J. Appl. Phys.* **111** 033527
- [132] Kim R H, Kim S, Song Y M, Jeong H, Kim T I, Lee J, Li X L, Choquette K D and Rogers J A 2012 Flexible vertical light emitting diodes *Small* **8** 3123–8
- [133] Lee H J *et al* 2009 Hydride vapor phase epitaxy of GaN on the vicinal c-sapphire with a CrN interlayer *J. Cryst. Growth* **311** 470–3
- [134] Ha J S, Lee S W, Lee H J, Lee H J, Lee S H, Goto H, Kato T, Fujii K, Cho M W and Yao T 2008 The fabrication of vertical light-emitting diodes using chemical lift-off process *IEEE Photonics Technol. Lett.* **20** 175–7
- [135] Meyer D J, Downey B P, Katzer D S, Nepal N, Wheeler V D, Hardy M T, Anderson T J and Storm D F 2016 Epitaxial lift-off and transfer of III-N materials and devices from SiC substrates *IEEE Trans. Semicond. Manuf.* **29** 384–9
- [136] Rajan A *et al* 2016 Wafer-scale epitaxial lift-off of optoelectronic grade GaN from a GaN substrate using a sacrificial ZnO interlayer *J. Phys. D: Appl. Phys.* **49** 315105
- [137] Rogers D J *et al* 2007 Use of ZnO thin films as sacrificial templates for metal organic vapor phase epitaxy and chemical lift-off of GaN *Appl. Phys. Lett.* **91** 071120
- [138] Wu F L, Ou S L, Kao Y C, Chen C L, Tseng M C, Lu F C, Lin M T and Horng R H 2015 Thin-film vertical-type AlGaInP LEDs fabricated by epitaxial lift-off process via the patterned design of Cu substrate *Opt. Express* **23** 18156–65
- [139] Hsueh H H, Ou S L, Wu D S and Horng R H 2015 InGaIn LED fabricated on Eco-GaN template with a Ga₂O₃ sacrificial layer for chemical lift-off application *Vacuum* **118** 8–12
- [140] Kim H S *et al* 2011 Unusual strategies for using indium gallium nitride grown on silicon (111) for solid-state lighting *Proc. Natl Acad. Sci. USA* **108** 10072–7
- [141] Lin M S, Lin C F, Huang W C, Wang G M, Shieh B C, Dai J J, Chang S Y, Wu D S, Liu P L and Horng R H 2011 Chemical-mechanical lift-off process for InGaIn epitaxial layers *Appl. Phys. Express* **4** 062101
- [142] Dorsaz J, Bühlmann H J, Carlin J F, Grandjean N and Ilegems M 2005 Selective oxidation of AlInN layers for current confinement in III-nitride devices *Appl. Phys. Lett.* **87** 072102
- [143] Wu F L, Ou S L, Horng R H and Kao Y C 2014 Improvement in separation rate of epitaxial lift-off by hydrophilic solvent for GaAs solar cell applications *Solar Energy Mater. Solar Cells* **122** 233–40
- [144] Kum H, Lee D, Kong W, Kim H, Park Y, Kim Y, Baek Y, Bae S H, Lee K and Kim J 2019 Epitaxial growth and layer-transfer techniques for heterogeneous integration of materials for electronic and photonic devices *Nat. Electron.* **2** 439–50
- [145] Chuang S H, Pan C T, Shen K C, Ou S L, Wu D S and Horng R H 2013 Thin film GaN LEDs using a patterned oxide sacrificial layer by chemical lift-off process *IEEE Photonics Technol. Lett.* **25** 2435–8

- [146] Chen L C, Wang C K, Huang J B and Hong L S 2009 A nanoporous AlN layer patterned by anodic aluminum oxide and its application as a buffer layer in a GaN-based light-emitting diode *Nanotechnology* **20** 085303
- [147] Anderson R, Cohen D, Mehari S, Nakamura S and DenBaars S 2019 Electrical injection of a 440nm InGaN laser with lateral confinement by nanoporous-GaN *Opt. Express* **27** 22764–9
- [148] Lin C F, Lee W C, Chen Y L, Tseng Y H, Dai J J and Han J 2014 Current confinement effect of InGaN devices by forming photoelectrochemical-oxidized GaN nanoporous structures *ECS Trans.* **61** 251–5
- [149] Li T T *et al* 2021 Epitaxial growth of wafer-scale molybdenum disulfide semiconductor single crystals on sapphire *Nat. Nanotechnol.* **16** 1201–7
- [150] Akamatsu T *et al* 2021 A van der Waals interface that creates in-plane polarization and a spontaneous photovoltaic effect *Science* **372** 68–72
- [151] Makimoto T, Kumakura K, Kobayashi Y, Akasaka T and Yamamoto H 2012 A vertical InGaN/GaN light-emitting diode fabricated on a flexible substrate by a mechanical transfer method using BN *Appl. Phys. Express* **5** 072102
- [152] Kobayashi Y, Kumakura K, Akasaka T and Makimoto T 2012 Layered boron nitride as a release layer for mechanical transfer of GaN-based devices *Nature* **484** 223–7
- [153] Qi Y *et al* 2018 Fast growth of strain-free AlN on graphene-buffered sapphire *J. Am. Chem. Soc.* **140** 11935–41
- [154] Leszczynski M *et al* 1996 Lattice parameters of gallium nitride *Appl. Phys. Lett.* **69** 73–75
- [155] Yu J D, Hao Z B, Wang L, Luo Y, Wang J, Sun C Z, Han Y J, Xiong B and Li H T 2021 First-principle calculations of adsorption of Ga (Al, N) adatoms on the graphene for the van-der-Waals epitaxy *Mater. Today Commun.* **26** 101571
- [156] Vuong P *et al* 2020 Control of the mechanical adhesion of III–V materials grown on layered h-BN *ACS Appl. Mater. Interfaces* **12** 55460–6
- [157] Kendall K 1975 Thin-film peeling-the elastic term *J. Phys. D: Appl. Phys.* **8** 1449–52
- [158] Chen Z L *et al* 2018 High-brightness blue light-emitting diodes enabled by a directly grown graphene buffer layer *Adv. Mater.* **30** 1801608
- [159] Chang H L *et al* 2019 Graphene-assisted quasi-van der Waals epitaxy of AlN film for ultraviolet light emitting diodes on nano-patterned sapphire substrate *Appl. Phys. Lett.* **114** 091107
- [160] Wang G X, Yang D Z, Zhang Z Y, Si M S, Xue D S, He H Y and Pandey R 2014 Decoding the mechanism of the mechanical transfer of a GaN-based heterostructure via an h-BN release layer in a device configuration *Appl. Phys. Lett.* **105** 121605
- [161] Wei Z X, Lin K, Wang X H and Zhao Y P 2021 Peeling of graphene/molybdenum disulfide heterostructure at different angles: a continuum model with accommodations for van der Waals interaction *Composites A* **150** 106592
- [162] Kim-Lee H J, Carlson A, Grierson D S, Rogers J A and Turner K T 2014 Interface mechanics of adhesiveless microtransfer printing processes *J. Appl. Phys.* **115** 143513
- [163] Luo A Y and Turner K T 2020 Mechanics of crack path selection in microtransfer printing: challenges and opportunities for process control *J. Mech. Phys. Solids* **143** 104066
- [164] Yoon J, Lee S M, Kang D, Meitl M A, Bower C A and Rogers J A 2015 Heterogeneously integrated optoelectronic devices enabled by micro-transfer printing *Adv. Opt. Mater.* **3** 1313–35
- [165] Wu W, Hu M, Ou F S, Li Z Y and Williams R S 2010 Cones sensitive surface enhanced Raman spectroscopy *Nanotechnology* **21** 255502
- [166] Igaku Y, Matsui S, Ishigaki H, Fujita J I, Ishida M, Ochiai Y, Namatsu H, Komuro M and Hiroshima H 2002 Room temperature nanoimprint technology using hydrogen silsequioxane (HSQ) *Jpn. J. Appl. Phys.* **41** 4198–202
- [167] Bhingardive V, Menahem L and Schwartzman M 2018 Soft thermal nanoimprint lithography using a nanocomposite mold *Nano Res.* **11** 2705–14
- [168] Fang Y, Yong J, Chen F, Huo J L, Yang Q, Zhang J Z and Hou X 2018 Bioinspired fabrication of Bi/tridirectionally anisotropic sliding superhydrophobic PDMS surfaces by femtosecond laser *Adv. Mater. Interfaces* **5** 1701245
- [169] Li M J, Yang Q, Chen F, Yong J L, Bian H, Wei Y, Fang Y and Hou X 2019 Integration of great water repellence and imaging performance on a superhydrophobic PDMS microlens array by femtosecond laser microfabrication *Adv. Eng. Mater.* **21** 1800994
- [170] Huang Y Y, Palocz G T, Scheuer J and Yariv A 2003 Soft lithography replication of polymeric microring optical resonators *Opt. Express* **11** 2452–8
- [171] Hassanin H, Mohammadkhani A and Jiang K 2012 Fabrication of hybrid nanostructured arrays using a PDMS/PDMS replication process *Lab Chip* **12** 4160–7
- [172] Sameoto D and Menon C 2009 Direct molding of dry adhesives with anisotropic peel strength using an offset lift-off photoresist mold *J. Micromech. Microeng.* **19** 115026
- [173] Jin K, Cremaldi J C, Erickson J S, Tian Y, Israelachvili J N and Pesika N S 2014 Biomimetic bidirectional switchable adhesive inspired by the gecko *Adv. Funct. Mater.* **24** 574–9
- [174] Tan D, Zheng Y J and Xue L J 2017 The role of effective elastic modulus in the performance of structured adhesives *Bio-Inspired Structured Adhesives* ed L Heepe, L J Xue and S N Gorb (Cham: Springer) pp 107–39
- [175] Tian Y, Pesika N, Zeng H B, Rosenberg K, Zhao B X, McGuiggan P, Autumn K and Israelachvili J 2006 Adhesion and friction in gecko toe attachment and detachment *Proc. Natl Acad. Sci. USA* **103** 19320–5
- [176] Hansen W R and Autumn K 2005 Evidence for self-cleaning in gecko setae *Proc. Natl Acad. Sci. USA* **102** 385–9
- [177] Zhou W, Huang Y, Menard E, Aluru N R, Rogers J A and Alleyne A G 2005 Mechanism for stamp collapse in soft lithography *Appl. Phys. Lett.* **87** 251925
- [178] Lakshminarayanan S 2018 Micro/nano patterning on polymers using soft lithography technique *Micro/Nanolithography: A Heuristic Aspect on the Enduring Technology* ed J Thirumalai (London: IntechOpen) p 69
- [179] Yang S Y *et al* 2012 Elastomer surfaces with directionally dependent adhesion strength and their use in transfer printing with continuous roll-to-roll applications *Adv. Mater.* **24** 2117–22
- [180] Cho S, Kim N, Song K and Lee J 2016 Adhesiveless transfer printing of ultrathin microscale semiconductor materials by controlling the bending radius of an elastomeric stamp *Langmuir* **32** 7951–7
- [181] Carlson A, Wang S D, Elvikis P, Ferreira P M, Huang Y G and Rogers J A 2012 Active, programmable elastomeric surfaces with tunable adhesion for deterministic assembly by transfer printing *Adv. Funct. Mater.* **22** 4476–84
- [182] Zhang W Q, Zhang L, Liao Y B and Cheng H Y 2021 Conformal manufacturing of soft deformable sensors on the curved surface *Int. J. Extremes Manuf.* **3** 042001
- [183] Huang Y A, Wu H, Xiao L, Duan Y Q, Zhu H, Bian J, Ye D and Yin Z P 2019 Assembly and applications of 3D conformal electronics on curvilinear surfaces *Mater. Horiz.* **6** 642–83

- [184] Huang Y, Zheng N, Cheng Z Q, Chen Y, Lu B W, Xie T and Feng X 2016 Direct laser writing-based programmable transfer printing via bioinspired shape memory reversible adhesive *ACS Appl. Mater. Interfaces* **8** 35628–33
- [185] Seo J, Eisenhaure J and Kim S 2016 Micro-wedge array surface of a shape memory polymer as a reversible dry adhesive *Extreme Mech. Lett.* **9** 207–14
- [186] Zhang S, Luo H Y, Wang S H, Chen Z, Nie S, Liu C Y and Song J Z 2021 A thermal actuated switchable dry adhesive with high reversibility for transfer printing *Int. J. Extremes Manuf.* **3** 035103
- [187] Cheng H Y, Wu J, Yu Q M, Kim-Lee H J, Carlson A, Turner K T, Hwang K C, Huang Y G and Rogers J A 2012 An analytical model for shear-enhanced adhesiveless transfer printing *Mech. Res. Commun.* **43** 46–49
- [188] Linghu C H, Zhang S, Wang C J, Yu K X, Li C L, Zeng Y J, Zhu H D, Jin X H, You Z Y and Song J Z 2020 Universal SMP gripper with massive and selective capabilities for multiscaled, arbitrarily shaped objects *Sci. Adv.* **6** eaay5120
- [189] Xue Y G, Zhang Y H, Feng X, Kim S, Rogers J A and Huang Y G 2015 A theoretical model of reversible adhesion in shape memory surface relief structures and its application in transfer printing *J. Mech. Phys. Solids* **77** 27–42
- [190] Linghu C H, Zhang S, Wang C J and Song J Z 2018 Transfer printing techniques for flexible and stretchable inorganic electronics *npj Flex. Electron.* **2** 26
- [191] Xia Y L, He Y, Zhang F H, Liu Y J and Leng J S 2021 A review of shape memory polymers and composites: mechanisms, materials, and applications *Adv. Mater.* **33** 2000713
- [192] Eisenhaure J and Kim S 2016 Laser-driven shape memory effect for transfer printing combining parallelism with individual object control *Adv. Mater. Technol.* **1** 1600098
- [193] Wu M H, Fang Y H and Chao C H 2017. Electric-programmable magnetic module and picking-up and placement process for electronic devices *U.S. Patent* No. 9607907
- [194] Chen L Y and Lee H W 2017 Method for transferring semiconductor structure *U.S. Patent* No. 9, 722, 134
- [195] De Volder M, Park S, Tawfick S and Hart A J 2014 Strain-engineered manufacturing of freeform carbon nanotube microstructures *Nat. Commun.* **5** 4512
- [196] Ahmad S, Copic D, George C and De Volder M 2016 Hierarchical assemblies of carbon nanotubes for ultraflexible li-ion batteries *Adv. Mater.* **28** 6705–10
- [197] Lee D H, Shin D O, Lee W J and Kim S O 2008 Hierarchically organized carbon nanotube arrays from self-assembled block copolymer nanotemplates *Adv. Mater.* **20** 2480–5
- [198] Shaw-Stewart J R H, Lippert T K, Nagel M, Nüesch F A and Wokaun A 2012 Sequential printing by laser-induced forward transfer to fabricate a polymer light-emitting diode pixel *ACS Appl. Mater. Interfaces* **4** 3535–41
- [199] Serra P and Piqué A 2019 Laser-induced forward transfer: fundamentals and applications *Adv. Mater. Technol.* **4** 1800099
- [200] Ehsani H, Boyd J D, Wang J L and Grady M E 2021 Evolution of the laser-induced spallation technique in film adhesion measurement *Appl. Mech. Rev.* **73** 030802
- [201] Nakata Y, Hayashi E, Tsubakimoto K, Miyanaga N, Narazaki A, Shoji T and Tsuboi Y 2020 Nanodot array deposition via single shot laser interference pattern using laser-induced forward transfer *Int. J. Extremes Manuf.* **2** 025101
- [202] Shaw Stewart J, Lippert T, Nagel M, Nüesch F and Wokaun A 2012 Red-green-blue polymer light-emitting diode pixels printed by optimized laser-induced forward transfer *Appl. Phys. Lett.* **100** 203303
- [203] Banks D P, Kaur K, Gazia R, Fardel R, Nagel M, Lippert T and Eason R W 2008 Triazene photopolymer dynamic release layer-assisted femtosecond laser-induced forward transfer with an active carrier substrate *EPL* **83** 38003
- [204] Shaw-Stewart J, Lippert T, Nagel M, Nüesch F and Wokaun A 2012 A simple model for flyer velocity from laser-induced forward transfer with a dynamic release layer *Appl. Surf. Sci.* **258** 9309–13
- [205] Mattle T, Shaw-Stewart J, Schneider C W, Lippert T and Wokaun A 2012 Laser induced forward transfer aluminum layers: process investigation by time resolved imaging *Appl. Surf. Sci.* **258** 9352–4
- [206] Fardel R, Nagel M, Nüesch F, Lippert T and Wokaun A 2010 Laser-induced forward transfer of organic LED building blocks studied by time-resolved shadowgraphy *J. Phys. Chem. C* **114** 5617–36
- [207] Shaw-Stewart J, Chu B, Lippert T, Maniglio Y, Nagel M, Nüesch F and Wokaun A 2011 Improved laser-induced forward transfer of organic semiconductor thin films by reducing the environmental pressure and controlling the substrate–substrate gap width *Appl. Phys. A* **105** 713–22
- [208] Feinaeugle M, Gregorčič P, Heath D J, Mills B and Eason R W 2017 Time-resolved imaging of flyer dynamics for femtosecond laser-induced backward transfer of solid polymer thin films *Appl. Surf. Sci.* **396** 1231–8
- [209] Rapp L, Constantinescu C, Larmande Y, Diallo A K, Videlot-Ackermann C, Delaporte P and Alloncle A P 2015 Functional multilayered capacitor pixels printed by picosecond laser-induced forward transfer using a smart beam shaping technique *Sens. Actuators A* **224** 111–8
- [210] Rapp L, Constantinescu C, Larmande Y, Alloncle A P and Delaporte P 2014 Smart beam shaping for the deposition of solid polymeric material by laser forward transfer *Appl. Phys. A* **117** 333–9
- [211] Goodfriend N T, Starinskiy S V, Nerushev O A, Bulgakova N M, Bulgakov A V and Campbell E E B 2016 Laser pulse duration dependence of blister formation on back-radiated Ti thin films for BB-LIFT *Appl. Phys. A* **122** 154
- [212] Brown M S, Kattamis N T and Arnold C B 2010 Time-resolved study of polyimide absorption layers for blister-actuated laser-induced forward transfer *J. Appl. Phys.* **107** 083103
- [213] Goodfriend N T *et al* 2018 Blister-based-laser-induced-forward-transfer: a non-contact, dry laser-based transfer method for nanomaterials *Nanotechnology* **29** 385301
- [214] Bian J, Chen F R, Yang B, Hu J L, Sun N N, Ye D, Duan Y Q, Yin Z P and Huang Y N G 2020 Laser-induced interfacial spallation for controllable and versatile delamination of flexible electronics *ACS Appl. Mater. Interfaces* **12** 54230–40
- [215] Lee J H, Loya P E, Lou J and Thomas E L 2014 Dynamic mechanical behavior of multilayer graphene via supersonic projectile penetration *Science* **346** 1092–6
- [216] Dong J L, Song X, Wang Z J, Xiao K L, Liu Y H, Wilde G, Wu X Q and Jiang M Q 2021 Impact resistance of single-layer metallic glass nanofilms to high-velocity micro-particle penetration *Extreme Mech. Lett.* **44** 101258
- [217] Hassani-Gangaraj M, Veysset D, Nelson K A and Schuh C A 2018 Melt-driven erosion in microparticle impact *Nat. Commun.* **9** 5077
- [218] Li R, Li Y H, F L C, Song J Z, Saeidpourazar R, Fang B, Zhong Y, Ferreira P M, Rogers J A and Huang Y G 2012 Axisymmetric thermo-mechanical analysis of laser-driven non-contact transfer printing *Int. J. Fract.* **176** 189–94

- [219] Saeidpourazar R, Li R, Li Y H, Sangid M D, Lu C F, Huang Y G, Rogers J A and Ferreira P M 2012 Laser-driven micro transfer placement of prefabricated microstructures *J. Microelectromech. Syst.* **21** 1049–58
- [220] Luo H Y, Wang C J, Linghu C H, Yu K X, Wang C and Song J Z 2020 Laser-driven programmable non-contact transfer printing of objects onto arbitrary receivers via an active elastomeric microstructured stamp *Nat. Sci. Rev.* **7** 296–304
- [221] Saeedi E, Kim S S, Etzkorn J R, Meldrum D R and Parviz B A 2007 Automation and yield of micron-scale self-assembly processes *Proc. 2007 IEEE Int. Conf. on Automation Science and Engineering* (Scottsdale, AZ: IEEE)
- [222] Kaltwasser M, Schmidt U, Lösing L, Biswas S, Stauden T, Bund A and Jacobs H O 2019 Fluidic self-assembly on electroplated multilayer solder bumps with tailored transformation imprinted melting points *Sci. Rep.* **9** 11325
- [223] Shet S, Revero R D, Booty M R, Fiory A T, Lepselter M P and Ravindra N M 2006 Microassembly techniques: a review *Materials Science & Technology 2006 Proc.* vol 451 (Cincinnati, Ohio: Materials Science & Technology)
- [224] Bohringer K F, Srinivasan U and Howe R T 2001 Modeling of capillary forces and binding sites for fluidic self-assembly *Proc. 14th IEEE Int. Conf. on Micro Electro Mechanical Systems* (Interlaken: IEEE) pp 369–74
- [225] Lin C, Tseng F G and Chieng C C 2009 Orientation-specific fluidic self-assembly process based on a capillary effect *J. Micromech. Microeng.* **19** 115020
- [226] Park S C, Biswas S, Fang J, Mozafari M, Stauden T and Jacobs H O 2015 Millimeter thin and rubber-like solid-state lighting modules fabricated using roll-to-roll fluidic self-assembly and lamination *Adv. Mater.* **27** 3661–8
- [227] Durniak M 2018 Methods and systems for parallel assembly, transfer, and bonding of ferromagnetic components *U.S. Patent* No. 20180261570
- [228] O’Riordan A, Redmond G, Dean T and Pez M 2003 Field-configured self-assembly: manufacturing at the mesoscale *Mater. Sci. Eng. C* **23** 3–6
- [229] O’Riordan A, Delaney P and Redmond G 2004 Field configured assembly: programmed manipulation and self-assembly at the mesoscale *Nano Lett.* **4** 761–5
- [230] Islam M S *et al* 2017 Towards 10 Gb/s orthogonal frequency division multiplexing-based visible light communication using a GaN violet micro-LED *Photon. Res.* **5** A35–A43
- [231] Khalid A M, Cossu G, Corsini R, Choudhury P and Ciaramella E 2012 1-Gb/s transmission over a phosphorescent white LED by using rate-adaptive discrete multitone modulation *IEEE Photon. J.* **4** 1465–73